Cosmic Rays observations near earth

Detection principles and measurements

 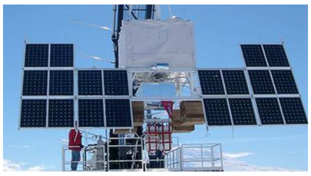 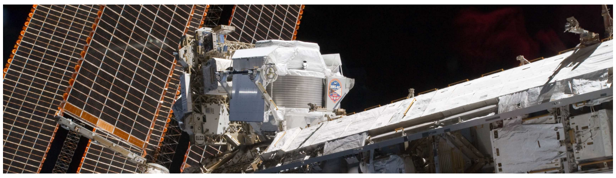

Fernando Barao (barao@lip.pt)
IST/LIP (+ LAPP)

Outline

- ✔ Cosmic rays and its detection environnment
  - historical perpective
  - spectra and composition
  - magnetosphere and heliosphere
- ✔ Cosmic rays detection in the ISS
  - AMS detector
  - detection principles and particle identification
- ✔ Physics results : e^+ ratio
  - positron identification
  - positron ratio results

Cosmic Rays

discovery, composition, spectra, rates

Cosmic rays : historical background

Before 1900 : the spontaneously ionization of air

Crookes (1879) : showed that an electrically charged object in a sealed container air-filled gradually looses its charge !

charge is retained if no air exists (vacuum)

1896 : the discovery of the radioactivity by Becquerel

This could explain the spontaneous discharge... !

1900-1910 : many observations were made ; among them **Pacini**, an italian metereologist, point evidences that ionization could have an origin independent of the direct action of radioactive substances contained in the upper layers of the earth crust.

Pacini's estimate of the excess ionization : 2 ion pairs $/cm^3/s$
corresponds to the ionization of cosmic rays at sea level !

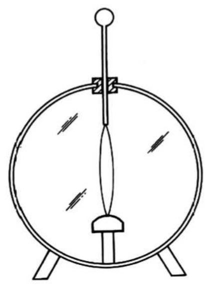

Fig. 6. Schematic view of the Wulf electrometer.

Cosmic rays : the Wulf measurement

The hypothesis of the earth surface radioactivity as ionization source suggested that measurements could be made in altitude.

one should detect a decrease in the intensity on this radiation and therefore an ionization decrease would be expected...

Jesuit priest Theodor Wulf (1910) : improved the electroscope replacing the gold leaves with two slender metal wires whose separation was measured with a microscope and carried it to the top of the Eiffel Tower (330 meters)

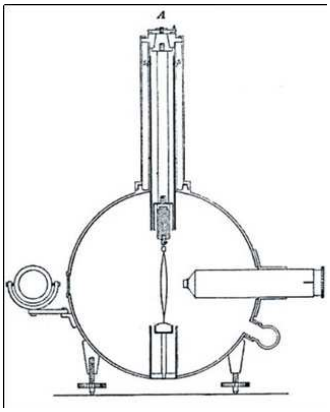

Datum	Ort	Ionen / ccm sec
28. März	Valkenburg	22,5
29. "	Paris, Boden	17,5
30. "	" Eiffelturm	16,2
31. "	" "	14,4
1. April	" "	15,0
2. "	" "	17,2
3. "	" Boden	18,3
4. "	Valkenburg	22,0

Daraus ergeben sich als Mittelwerte für die drei Orte

Valkenburg	22,25	Ionen / ccm · sec
Paris Boden	18,0	"
Paris Eiffelturm . .	15,7	"

Measured ionization rate at the Tower summit
15.7 ± 1.3 ions/cc/s
3.5 after bck subtraction
$\Rightarrow 60\%$ reduction

a small decrease when compared with the Wulf predictions
$\sim 1\%$

Cosmic rays : Hess discovery

Gockel, 1909-1911 : swiss physicist flew electrometers on balloon flights to 2500 and 2800m

no significant variation of the ionization rate recorded

Hess, 1911-1912 : austrian physicist made several ballloon flights

last flight took place on 7 August 1912 in a hydrogen-filled balloon. It lasted 6 hours and reached the altitude of 5350m.

three Wulf electrometers carried, 2 at atmospheric pressure and one opened

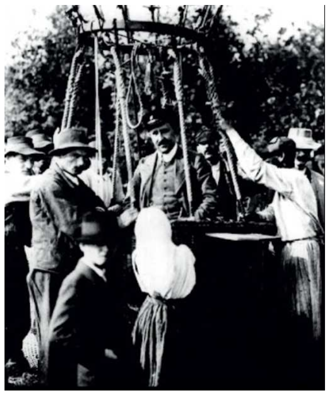

Balloon "Böhmen" (1680 cbm hydrogen) Leader: Captain W. Hoffory.
Meteorological observer: E. Wolf. Electr. observer: V. F. Hess

No.	Time	Mean height abs. m	Mean height rel. m	Observed radiation Inst. 1 q_1	Observed radiation Inst. 2 q_2	Inst. 3 q_3	Inst. 3 red. q_3	Temp.	Rel. humidity %
1	$15^h 15$–$16^h 15$	156	0	17.3	12.9	···	···	$1\frac{1}{2}$ days before the ascent (in Vienna)	
2	$16^h 15$–$17^h 15$	156	0	15.9	11.0	18.4	18.4		
3	$17^h 15$–$18^h 15$	156	0	15.8	11.2	17.5	17.5		
4	$6^h 45$–$7^h 45$	1700	1400	15.8	14.4	21.1	25.3	$+6.4°$	60
5	$7^h 45$–$8^h 45$	2750	2500	17.3	12.3	22.5	31.2	$+1.4°$	41
6	$8^h 45$–$9^h 45$	3850	3600	19.8	16.5	21.8	35.2	$-6.8°$	64
7	$9^h 45$–$10^h 45$	4800 (4400–5350)	4700	40.7	31.8	(ended by accident)		$-9.8°$	40
8	$10^h 45$–$11^h 15$	4400	4200	28.1	22.7			···	···
9	$11^h 15$–$11^h 45$	1300	1200	(9.7)	11.5			···	···
10	$11^h 45$–$12^h 10$	250	150	11.9	10.7			$+16.0°$	68
11	$12^h 25$–$13^h 12$	140	0	15.0	11.6	(After landing at Pieskow, Brandenburg)			

Cosmic rays : Hess discovery

Gockel, 1909-1911 : swiss physicist flew electrometers on balloon flights to 2500 and 2800m

no significant variation of the ionization rate recorded

Hess, 1911-1912 : austrian physicist made several ballloon flights

last flight took place on 7 August 1912 in a hydrogen-filled balloon. It lasted 6 hours and reached the altitude of 5350m.

three Wulf electrometers carried, 2 at atmospheric pressure and one opened

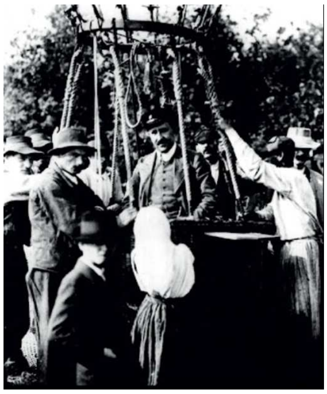

Balloon "Böhmen" (1680 cbm hydrogen)
Meteorological observer: E. Wolf.

Leader: Captain W. Hoffory.
Electr. observer: V. F. Hess

No.	Time	Mea…		Observed radiation Inst. 1 q_1	Inst. 2 q_2	Inst. 3 q_3	Inst. 3 red. q_3	Temp.	Rel. humidity %
1	15^h 15–16^h…	[illegible]	0	17.3	12.9	···	···	$1\frac{1}{2}$ days before the ascent (in Vienna)	
2	16^h 1…	[illegible]	0	15.9	11.0	18.4	18.4		
3	1…	[illegible]	0	15.8	11.2	17.5	17.5		
4	[illegible]	…00	1400	15.8	14.4	21.1	25.3	+ 6.4°	60
5	[illegible]	2750	2500	17.3	12.3	22.5	31.2	+ 1.4°	41
6	[illegible]	3850	3600	19.8	16.5	21.8	35.2	− 6.8°	64
[illegible]	[illegible]	4800 (4400–5350)	4700	40.7	31.8	(ended by accident)		− 9.8°	40
8	…–11^h 15	4400	4200	28.1	22.7			···	···
9	11^h 15–11^h 45	1300	1200	(9.7)	11.5			···	···
10	11^h 45–12^h 10	250	150	11.9	10.7			+ 16.0°	68
11	12^h 25–13^h 12	140	0	15.0	11.6	(After landing at Pieskow, Brandenburg)			

clear increase from 2500m on !

Cosmic rays : Hess discovery

Gockel, 1909-1911 : swiss physicist flew electrometers on balloon flights to 2500 and 2800m

no significant variation of the ionization rate recorded

Hess, 1911-1912 : austrian physicist made several ballloon flights

last flight took place on 7 August 1912 in a hydrogen-filled balloon. It lasted 6 hours and reached the altitude of 5350m.

three Wulf electrometers carried, 2 at atmospheric pressure and one opened

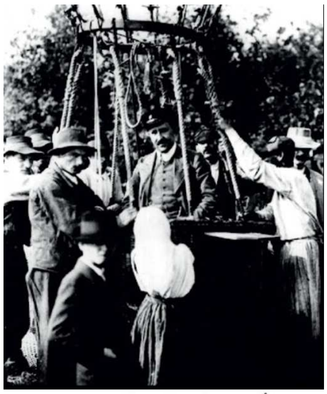

Balloon "Böhmen" (1680 cbm hydrogen)
Meteorological observer: E. Wolf.

Leader: Captain W. Hoffory.
Electr. observer: V. F. Hess

No.	Time	Mea…		Observed radiation Inst. 1 q_1	Inst. 2 q_2	Inst. 3 q_3	Inst. 3 red. q_3	Temp.	Rel. humidity %
1	15^h 15–16^h…	[illegible]	0	17.3	12.9	···	···	$1\frac{1}{2}$ days before the ascent (in Vienna)	
2	16^h 1…	[illegible]	0	15.9	11.0	18.4	18.4		
3	1…	[illegible]	0	15.8	11.2	17.5	17.5		
4	[illegible]	…00	1400	15.8	14.4	21.1	25.3	+ 6.4°	60
5	[illegible]	2750	2500	17.3	12.3	22.5	31.2	+ 1.4°	41
6	[illegible]	3850	3600	19.8	16.5	21.8	35.2	− 6.8°	64
[illegible]	[illegible]	4800 (4400–5350)	4700	40.7	31.8	(ended by accident)		− 9.8°	40
8	…–11^h 15	4400	4200	28.1	22.7			···	···
9	11^h 15–11^h 45	1300	1200	(9.7)	11.5			···	···
10	11^h 45–12^h 10	250	150	11.9	10.7			+ 16.0°	68
11	12^h 25–13^h 12	140	0	15.0	11.6	(After landing at Pieskow, Brandenburg)			

clear increase from 2500m on !

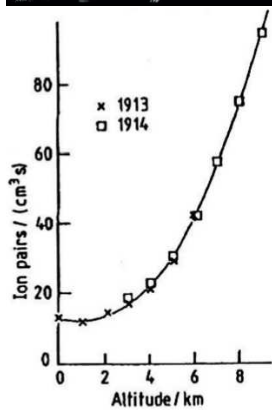

Kolhorster flights (1913-1914) confirmed !

Cosmic rays : positron (e^+) discovery

Carl Anderson, 1932 : finding the positron...

- ✔ Detector : cloud chamber and a high magnetic field ($\vec{B} \sim 2.5\ T$)
- ✔ charged particles are defleclted on the magnetic field depending on their charge sign

  $\boxed{\text{Lorentz force : } \vec{F} = \pm q\ \vec{v} \times \vec{B}}$
- ✔ the particle momentum can be measured from the track curvature

Cosmic rays : positron (e^+) discovery

Carl Anderson, 1932 : finding the positron...


© Copyright California Institute of Technology. All rights reserved.
Commercial use or modification of this material is prohibited.

- ✔ Detector : cloud chamber and a high magnetic field ($\vec{B} \sim 2.5\ T$)
- ✔ charged particles are defleclted on the magnetic field depending on their charge sign

  $\boxed{\text{Lorentz force : } \vec{F} = \pm q\ \vec{v} \times \vec{B}}$
- ✔ the particle momentum can be measured from the track curvature

What was expected to observe ?

- ✔ Millikan was convinced that the primary cosmic rays were high energy photons !
- ✔ one would expect to see Compton electrons (photons interact with the electrons of the atom and eject them)

Cosmic rays : positron (e^+) discovery

Carl Anderson, 1932 : finding the positron...

- Detector : cloud chamber and a high magnetic field ($\vec{B} \sim 2.5\ T$)
- charged particles are defleclted on the magnetic field depending on their charge sign

  Lorentz force : $\vec{F} = \pm q\ \vec{v} \times \vec{B}$
- the particle momentum can be measured from the track curvature

What was expected to observe ?

- Millikan was convinced that the primary cosmic rays were high energy photons !
- one would expect to see Compton electrons (photons interact with the electrons of the atom and eject them)

...but positive and negative tracks were observed !

Cosmic rays : positron (e^+) discovery

positron identification

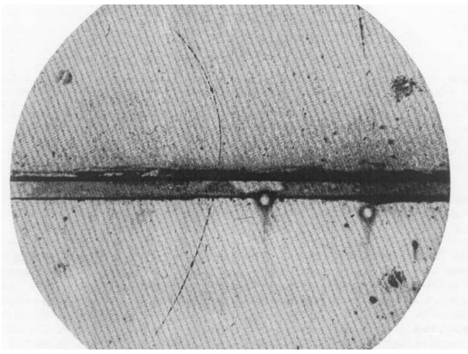

- the positron and proton curvature were similar (both are positive particles)
- for similar curvature particles (same momentum !) the energy deposited by the slowest particles (proton) is larger

  $$dE/dx \propto 1/\beta^2 \propto \left[1 + \left(\frac{m}{p}\right)^2\right]$$

  proton tracks shall be thicker as the density of droplets is larger

Cosmic rays : positron (e^+) discovery

positron identification

- the positron and proton curvature were similar (both are positive particles)
- for similar curvature particles (same momentum !) the energy deposited by the slowest particles (proton) is larger

$$dE/dx \propto 1/\beta^2 \propto \left[1 + \left(\frac{m}{p}\right)^2\right]$$

proton tracks shall be thicker as the density of droplets is larger

- negative tracks from below and positive particle entering from above have similar curvature

Anderson inserted a lead plate in the cloud chamber to distinguish particle direction !

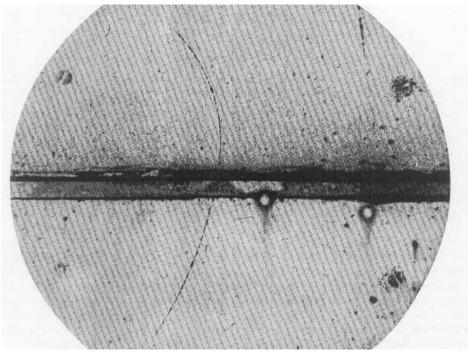

Cosmic rays : positron (e^+) discovery

positron identification

- the positron and proton curvature were similar (both are positive particles)
- for similar curvature particles (same momentum !) the energy deposited by the slowest particles (proton) is larger

$$dE/dx \propto 1/\beta^2 \propto \left[1 + \left(\frac{m}{p}\right)^2\right]$$

proton tracks shall be thicker as the density of droplets is larger

- negative tracks from below and positive particle entering from above have similar curvature

Anderson inserted a lead plate in the cloud chamber to distinguish particle direction !

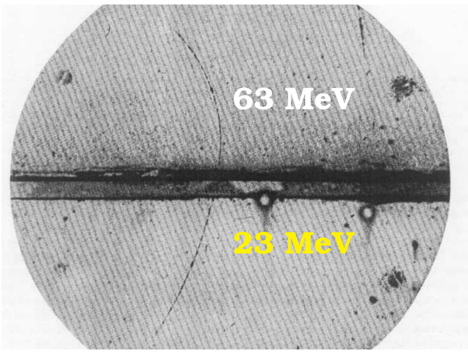

Cosmic rays : positron (e^+) discovery

positron identification

- ✔ the positron and proton curvature were similar (both are positive particles)
- ✔ for similar curvature particles (same momentum !) the energy deposited by the slowest particles (proton) is larger

  $$\boxed{dE/dx \propto 1/\beta^2 \propto \left[1 + \left(\frac{m}{p}\right)^2\right]}$$

  proton tracks shall be thicker as the density of droplets is larger
- ✔ negative tracks from below and positive particle entering from above have similar curvature
  Anderson inserted a lead plate in the cloud chamber to distinguish particle direction !

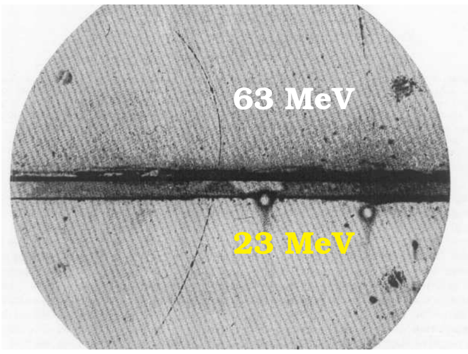

The Positive Electron

CARL D. ANDERSON,
California Institute of Technology, Pasadena, California

(Received February 28, 1933)

Abstract

Out of a group of 1300 photographs of cosmic-ray tracks in a vertical Wilson chamber 15 tracks were of positive particles which could not have a mass as great as that of the proton. From an examination of the energy-loss and ionization produced it is concluded thai the charge is less than twice, and is probably exactly equal to, that of the proton. If these particles carry unit positive charge the curvatures and ionizations produced require the mass to be less than twenty times the electron mass. These particles will be called positrons. Because they occur in groups associated with other tracks it is concluded that they must be secondary particles ejected from atomic nuclei.

It had : track thickness compatible with a positron (electron) and it was entering from above ! **So it was a positive electron !**

Cosmic rays : what are they ?

A very interesting probe...

- ✔ evidence of very powerful astrophysical accelerators
  their energy spans over ~ 20 orders of magnitude
- ✔ provides information about the cosmic environment
  halo size, heliosphere and magnetosphere
- ✔ can indirectly probe the dark matter nature
- ✔ probe primordial antimatter (antinuclei !)
- ✔ ...and other new physics !

Cosmic rays : what are they ?

A very interesting probe...

- ✔ evidence of very powerful astrophysical accelerators
  their energy spans over ~ 20 orders of magnitude
- ✔ provides information about the cosmic environment
  halo size, heliosphere and magnetosphere
- ✔ can indirectly probe the dark matter nature
- ✔ probe primordial antimatter (antinuclei !)
- ✔ ...and other new physics !

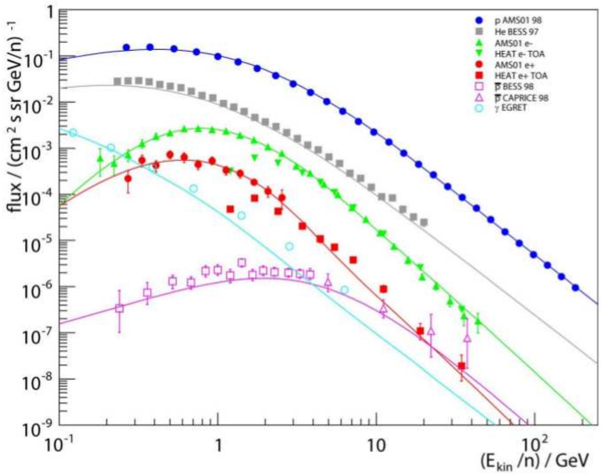

CRs	abundance @ 10 GeV
protons	88%
helium	10%
electrons	1%
positrons	0.1%
gammas	0.01%
antiprotons	0.001%

Cosmic rays : abundances

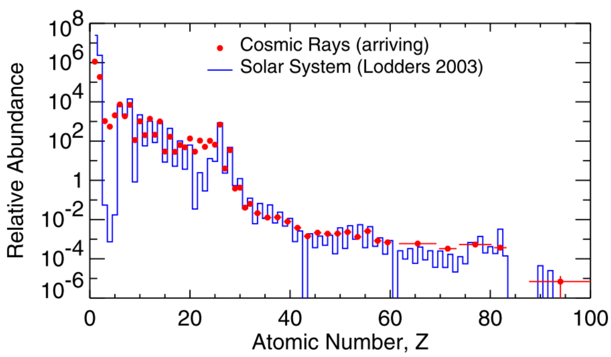

- ✔ similar features on solar and cosmic rays abundances
  similar nucleosynthesis processes
- ✔ some elements result from CRs interactions with the interstellar medium (spallation)
  (Li,Be,B) on CRs from C,O spallation
  (Sc,V,Mn) on CRs from Fe spallation
- ✔ synthesis of elements havier than Iron steeps down

Cosmic rays : abundances

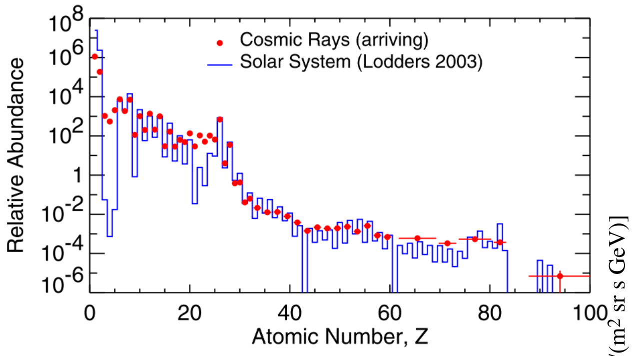

- ✔ similar features on solar and cosmic rays abundances
  similar nucleosynthesis processes
- ✔ some elements result from CRs interactions with the interstellar medium (spallation)
  (Li,Be,B) on CRs from C,O spallation
  (Sc,V,Mn) on CRs from Fe spallation
- ✔ synthesis of elements havier than Iron steeps down

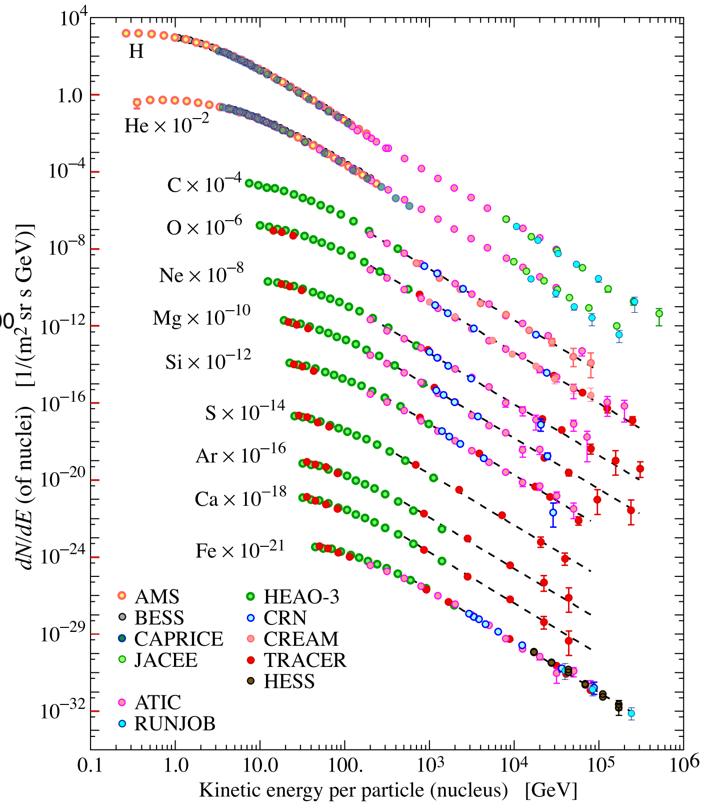

Cosmic rays : detection

- ✔ earth atmosphere represents a thickness of
  $t = \int_z \rho(z)dz \sim 1000\ g.cm^{-2}$
  11.5 nuclear interactions lengths
  28 radiation lengths
- ✔ primary cosmic rays will undergo nuclear and electromagntic interactions, producing a lot of secondary particles : pions, kaons, neutrons, electrons, muons, photons neutrinos,...

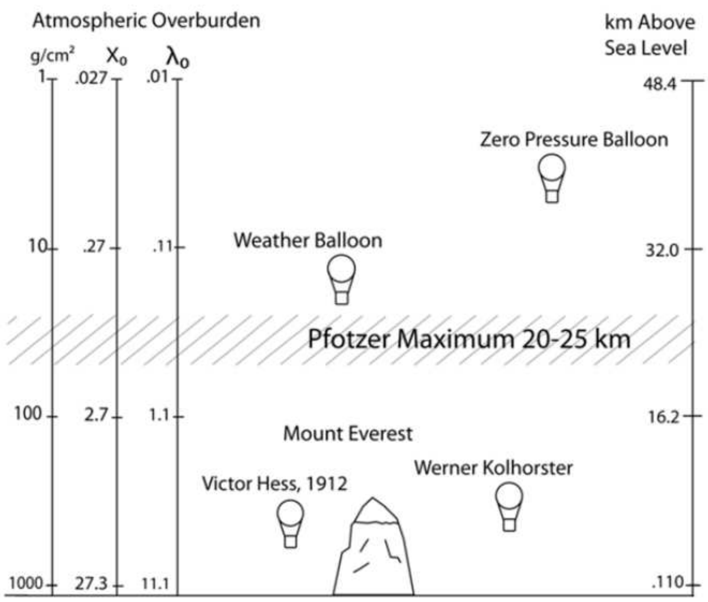

Cosmic rays : detection

Detection of
primary cosmic rays
require detectors to be
installed
above atmosphere !


ISS


AMS


Pamela

- earth atmosphere represents a thickness of
  $t = \int_z \rho(z)dz \sim 1000\ g.cm^{-2}$
  11.5 nuclear interactions lengths
  28 radiation lengths
- primary cosmic rays will undergo nuclear and electromagntic interactions, producing a lot of secondary particles : pions, kaons, neutrons, electrons, muons, photons, neutrinos,...

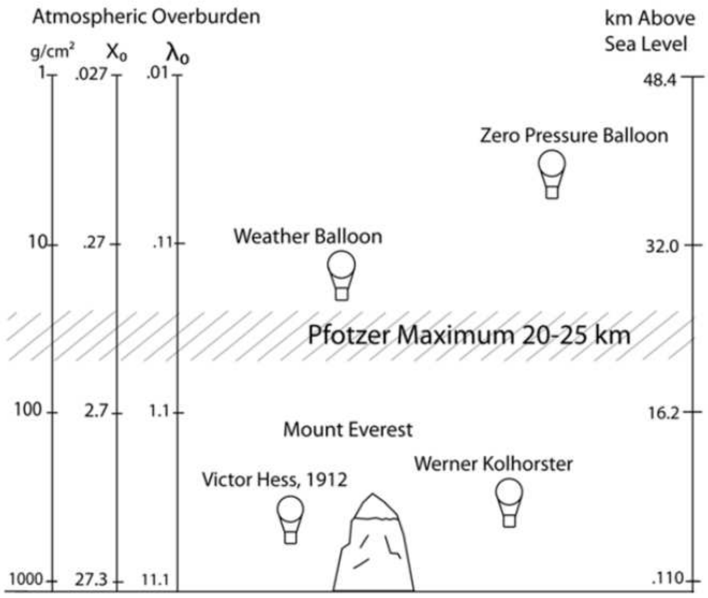

Cosmic rays : direct detection

- direct detection of primary cosmic rays implies the transport of detectors to at least 30 km from earth
- beginning of 1930's very short flights on balloon (< 1h) could reach 30 Km
  Vernov, 1934 : Geiger-Muller counters in coincidence

Cosmic rays : direct detection

- ✔ direct detection of primary cosmic rays implies the transport of detectors to at least 30 km from earth
- ✔ beginning of 1930's very short flights on balloon (< 1h) could reach 30 Km
  Vernov, 1934 : Geiger-Muller counters in coincidence
- ✔ 1948 : V2 rocket instrumented with Geiger-Mullet counters made a ballistic flight
  first cosmic ray intensity profiles measured until 150 Km

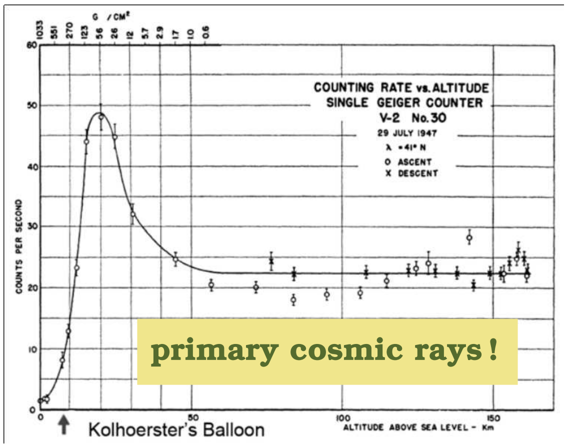

Cosmic rays : direct detection

- ✔ direct detection of primary cosmic rays implies the transport of detectors to at least 30 km from earth
- ✔ beginning of 1930's very short flights on balloon (< 1h) could reach 30 Km
  Vernov, 1934 : Geiger-Muller counters in coincidence
- ✔ 1948 : V2 rocket instrumented with Geiger-Mullet counters made a ballistic flight
  first cosmic ray intensity profiles measured until 150 Km
- ✔ "Zero-Pressure" balloons developed in the late 1940's could carry several tons detectors to altitudes of 30 to 45 Km
  few days flight
- ✔ long-duration balloon flights
  several weeks flight

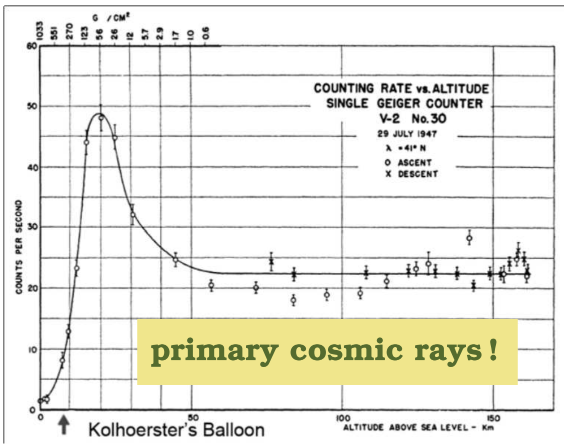

Geomagnetic Field

configuration, implications

Geomagnetic field

the earth has a magnetic field - geomagnetic field

the zone of influence is called the **magnetosphere**

- ✔ main source : inside earth, there are electrical currents related to the rotating metallic nucleus
- ✔ outer sources : ionosphere currents, ring current (charged particles trapped in radiation belts)

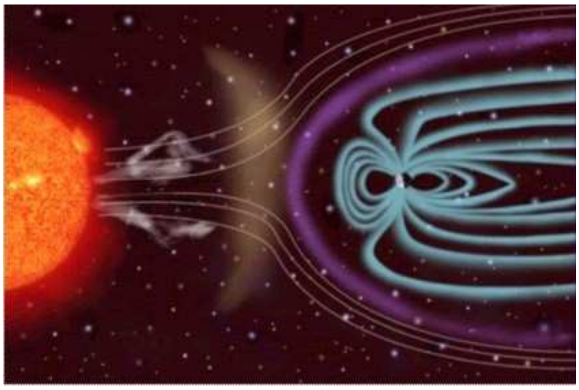

as a first approximation it can be represented by a magnetic dipole

- ✔ the geomagnetic equator is tilted 11.5^o wrt geographic equator
- ✔ not centered with earth *(eccentric dipole)*

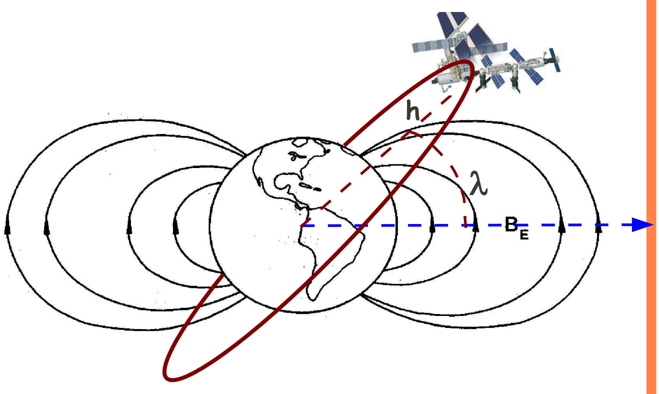

more complete model
IGRF + magnetospheric field model

Geomagnetic field : dipolar approx

potencial vector

$\vec{A} = \frac{\mu_0}{4\pi} I \oint_C \frac{d\vec{\ell}}{r} = \frac{\mu_0}{4\pi}\frac{M}{r^2}\cos\lambda\,\vec{e}_\Phi$

earth dipolar moment

$M = 7.73\ 10^{22}\ A.m^2$ (2013)

magnetic field

$\vec{B} = \vec{\nabla}\times\vec{A} = \frac{\mu_0}{4\pi}\frac{M}{r^3}\left(\cos\lambda\vec{e}_\lambda - 2\sin\lambda\vec{e}_r\right)$

$\left|\vec{B}\right| = \frac{\mu_0}{4\pi}\frac{M}{r^3}\sqrt{1+3\sin^2\lambda}$

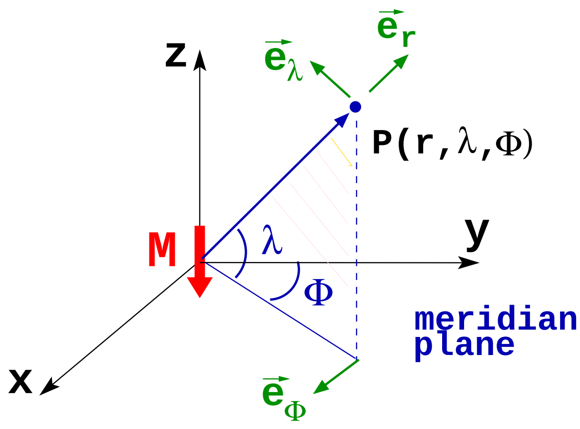

Geomagnetic field : dipolar approx

potencial vector

$\vec{A} = \frac{\mu_0}{4\pi} I \oint_C \frac{d\vec{\ell}}{r} = \frac{\mu_0}{4\pi}\frac{M}{r^2}\cos\lambda\,\vec{e}_\Phi$

earth dipolar moment

$M = 7.73\ 10^{22}\ A.m^2$ (2013)

magnetic field

$\vec{B} = \vec{\nabla}\times\vec{A} = \frac{\mu_0}{4\pi}\frac{M}{r^3}\left(\cos\lambda\vec{e}_\lambda - 2\sin\lambda\vec{e}_r\right)$

$\left|\vec{B}\right| = \frac{\mu_0}{4\pi}\frac{M}{r^3}\sqrt{1+3\sin^2\lambda}$

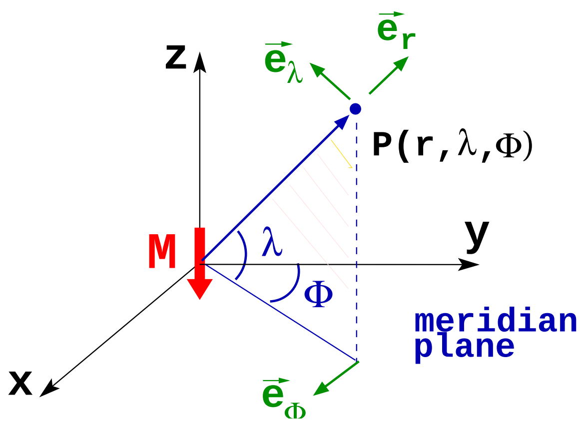

B at the ISS

$r = R_E + 400$ Km

$B = 26\sqrt{1+3\sin^2\lambda}\ [\mu T]$

$\quad = 0.26\sqrt{1+3\sin^2\lambda}\ [G]$

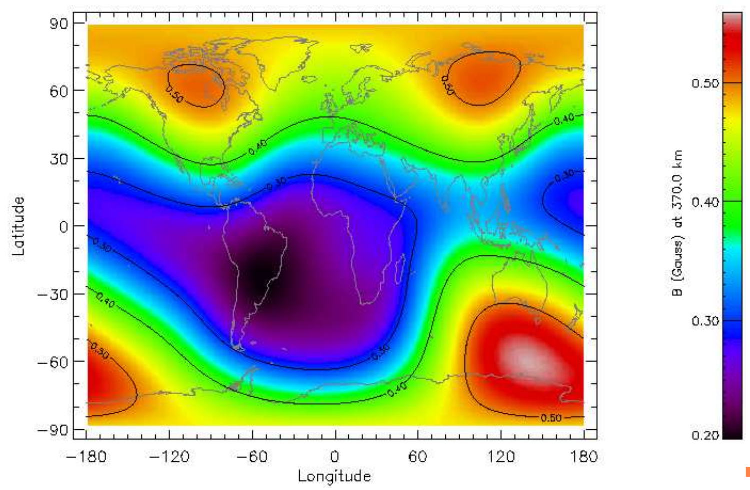

Geomagnetic field : particle motion

equatorial field ($\lambda = 0$)

$$B = \frac{\mu_0}{4\pi}\frac{M}{r^3}$$

particle trajectory and orbit

$$\begin{cases} zvB = \gamma m \frac{v^2}{r} \\ B = \frac{\mu_0}{4\pi}\frac{M}{r^3} \end{cases} \Rightarrow r^{-2} = \frac{p}{ze}\frac{1}{M}\frac{4\pi}{\mu_0}$$

momentum corresponding to orbit R_E

$$p_E = \frac{\mu_0}{4\pi} M \frac{ze}{R_E^2} \underbrace{\left(c\frac{10^{-9}}{e}\right)}_{J \rightarrow GeV} = 57\ z\ [GeV/c]$$

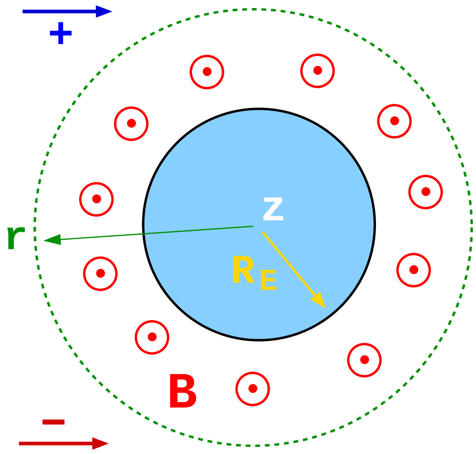

Geomagnetic field : particle motion

equatorial field ($\lambda = 0$)

$$B = \frac{\mu_0}{4\pi}\frac{M}{r^3}$$

particle trajectory and orbit

$$\begin{cases} zvB = \gamma m \frac{v^2}{r} \\ B = \frac{\mu_0}{4\pi}\frac{M}{r^3} \end{cases} \Rightarrow r^{-2} = \frac{p}{ze}\frac{1}{M}\frac{4\pi}{\mu_0}$$

momentum corresponding to orbit R_E

$$p_E = \frac{\mu_0}{4\pi} M \frac{ze}{R_E^2} \underbrace{\left(c\frac{10^{-9}}{e}\right)}_{J \rightarrow GeV} = 57\ z\ [GeV/c]$$

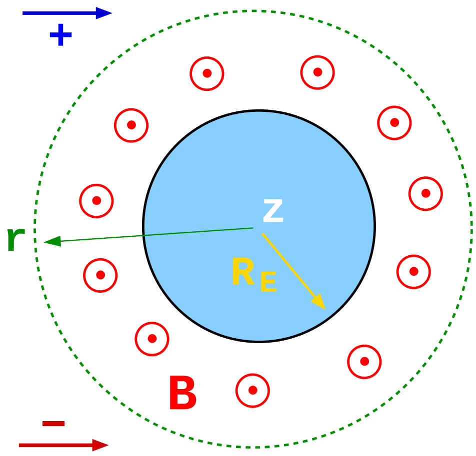

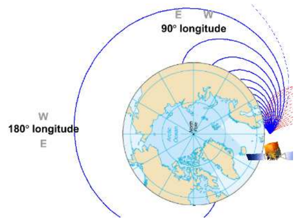

particles with rigidities larger than 57 GV have orbits radius larger than R_E and are therefore relatively unaffected by the geomagnetic field

rigidity P

$$P_E = \frac{p_E c}{ze} = 57\ GV$$

Geomagnetic field : rigidity cutoff

The rigidity cutoff is the minimal rigidity of a particle coming from infinity which can reach an observer in a point $P(r, \lambda, \Phi)$ and having a velocity $\vec{v}$
it measures the shielding provided by the earth's magnetic field

The trajectory of particles moving in the earth's magnetic field were initiated by C. Stormer (1930's) to understand the polar aurora phenomenon

Lorentz equation

$$\left\{ \begin{array}{lll} \frac{d\vec{p}}{dt} & = & \gamma m \vec{a} \\ \vec{F}_B & = & z e \vec{v} \times \vec{B} \quad \text{(v const)} \end{array} \right.$$

spherical coordinates
position : $\vec{r} = r\vec{e}_r$
velocity : $\vec{r} = \dot{r}\vec{e}_r + \dot{\lambda} r \vec{e}_\lambda + r\dot{\Phi}\cos\lambda \vec{e}_\Phi$

Geomagnetic field : rigidity cutoff

The rigidity cutoff is the minimal rigidity of a particle coming from infinity which can reach an observer in a point $P(r, \lambda, \Phi)$ and having a velocity $\vec{v}$
it measures the shielding provided by the earth's magnetic field

The trajectory of particles moving in the earth's magnetic field were initiated by C. Stormer (1930's) to understand the polar aurora phenomenon

Lorentz equation

$$\left\{ \begin{array}{lll} \frac{d\vec{p}}{dt} & = & \gamma m \vec{a} \\ \vec{F}_B & = & z e \vec{v} \times \vec{B} \quad \text{(v const)} \end{array} \right.$$

spherical coordinates
position : $\vec{r} = r\vec{e}_r$
velocity : $\vec{r} = \dot{r}\vec{e}_r + \dot{\lambda} r \vec{e}_\lambda + r\dot{\Phi}\cos\lambda \vec{e}_\Phi$

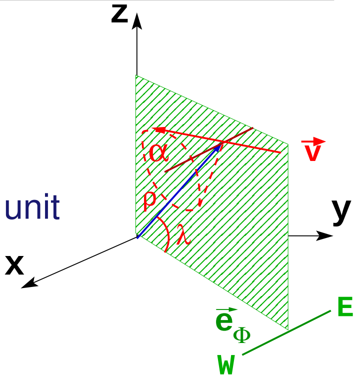

$$\gamma\, m \begin{pmatrix} a_r \\ a_\lambda \\ a_\Phi \end{pmatrix} = \frac{\mu_0}{4\pi}\ \frac{M}{r^3} \begin{pmatrix} \dot{r} \\ r\dot{\lambda} \\ r\cos\lambda\dot{\Phi} \end{pmatrix} \times \begin{pmatrix} -2\sin\lambda \\ \cos\lambda \\ 0 \end{pmatrix}$$

as p_Φ is a constant of the motion and using stormer "length" unit $\left[s = \sqrt{\frac{\mu_0}{4\pi}\frac{M c}{P}} \right]$, one defines $\rho = r/s = \frac{r}{R_E}\sqrt{P/P_E}$:

$\boxed{\rho\cos\lambda\cos\alpha + \frac{z}{|z|}\frac{\cos^2\lambda}{\rho} = C}$ $|\cos\alpha| = \frac{C}{\rho\cos\lambda} - \frac{z}{|z|}\frac{\cos\lambda}{\rho^2} \leq 1$

C, ρ, λ constrained by inequality ; allowed trajectories have : $|C| < 2$

Geomagnetic field : rigidity cutoff

- ✔ Using the allowed trajectories condition $C=2$, one can solve the previous equation and get the minimal adimensional distance $\rho_c(\lambda,\alpha)$
- ✔ this can be translated to rigidity : $P_c = P_E\ \left(\frac{R_E}{r}\right)^2\ \rho_c^2$, where $P_E = 57\ GV$ (2013 dipole) is the particle rigidity providing a curvature radius equal to R_E

$$\boxed{P_c = P_E \left(\frac{R_E}{r}\right)^2 \frac{\cos^4\lambda}{\left[1+\left(1-\frac{z}{|z|}\cos\alpha\cos^3\lambda\right)^{1/2}\right]^2}}$$

Geomagnetic field : rigidity cutoff

- ✔ Using the allowed trajectories condition $C=2$, one can solve the previous equation and get the minimal adimensional distance $\rho_c(\lambda,\alpha)$
- ✔ this can be translated to rigidity : $P_c = P_E\ \left(\frac{R_E}{r}\right)^2\ \rho_c^2$, where $P_E = 57\ GV$ (2013 dipole) is the particle rigidity providing a curvature radius equal to R_E

$$\boxed{P_c = P_E \left(\frac{R_E}{r}\right)^2 \frac{\cos^4\lambda}{\left[1+\left(1-\frac{z}{|z|}\cos\alpha\cos^3\lambda\right)^{1/2}\right]^2}}$$

east-west effect at earth (for $+$ particles)

equatorial plane : $\lambda = 0$

arriving from eastern horizon ($\alpha = 0$) : $P_c = P_E$

arriving from western horizon ($\alpha = 180$) : $P_c \simeq P_E/6$

more positive particles arrive from W than from E !

$$\frac{N_{east}}{N_{west}} = \left(\frac{P_c(\alpha=0)}{P_c(\alpha=180)}\right)^{1-2.7} \sim 6^{-1.7} \sim 1/20$$

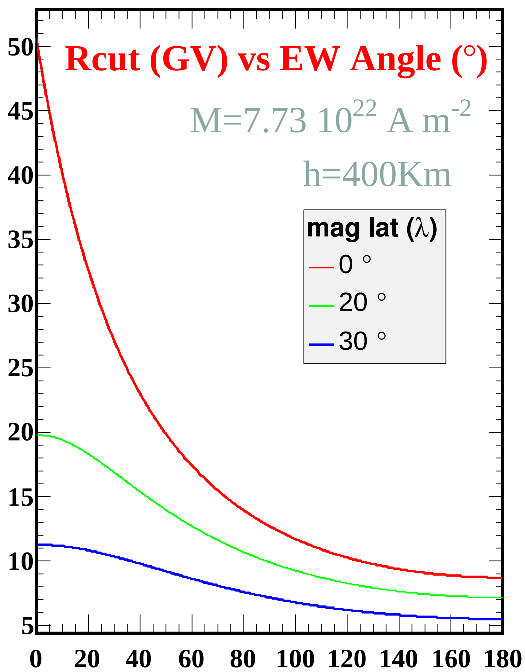

the nature of cosmic rays

- ✔ Until the end of 1920s was not clear if cosmic rays were charged or neutral (γ rays) particles
  Millikan and Compton dispute !

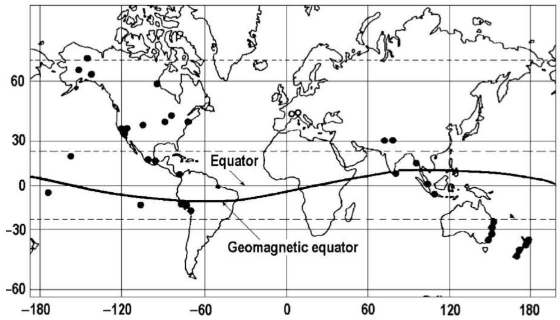

the nature of cosmic rays

- ✔ Until the end of 1920s was not clear if cosmic rays were charged or neutral (γ rays) particles
  Millikan and Compton dispute !

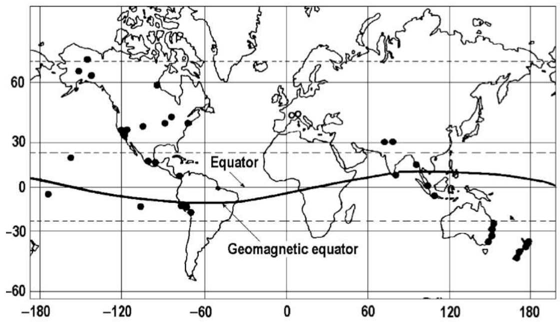

- ✔ The geomagnetic effect in cosmic rays was observed in 1927 by J. Clay, using an ionization chamber when travelling from Java island to Holland (*Slamat* ship)
- ✔ In 1932, Compton organized eight expeditions for cosmic ray intensity measurements at several locations (latitude and longitude different)
  a clear dependence with the latitude was observed providing the charged nature of the cosmic rays !

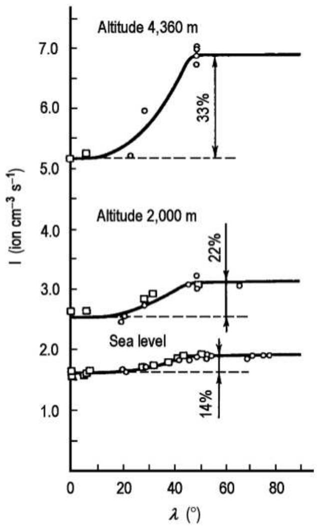

AMS02 proton rates

- ✔ AMS is installed in the International Space Station and orbiting around earth
- ✔ it is continously passing through different magnetic latitudes (λ)

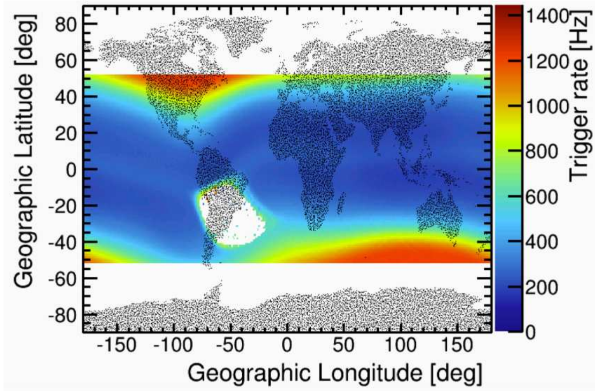

AMS02 proton rates

- ✔ AMS is installed in the International Space Station and orbiting around earth
- ✔ it is continously passing through different magnetic latitudes (λ)

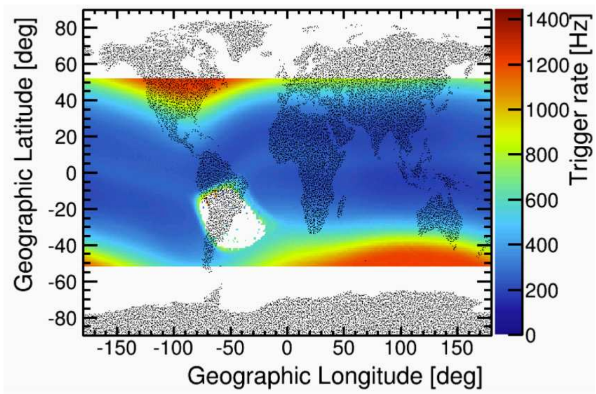

- ✔ measuring particle rates

$$\frac{dRate}{dE} = \frac{d}{dE}\frac{dN}{dt} = \frac{1}{T_\lambda}\frac{\Delta N(E)}{\Delta E}$$

detected proton rates measured at different geomagnetic latitudes drop at the rigidity cutoff values

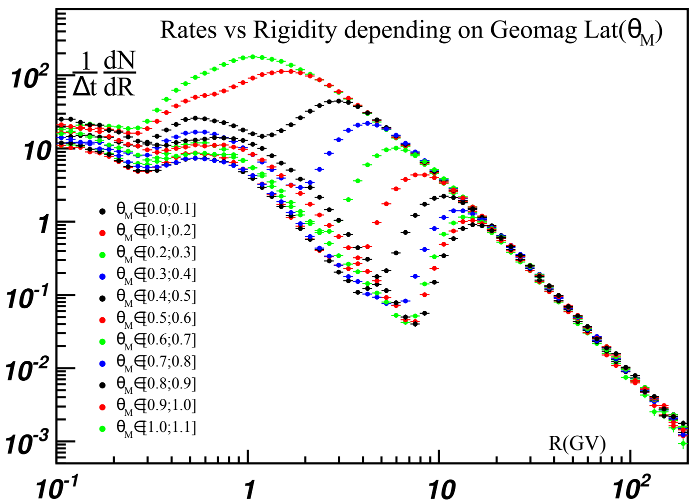

Solar Modulation

sun activity, flares, propagation

Heliosphere

- A region of space influenced by the sun and its expanding **Corona** : solar wind
  - *size : 100-150 AU*
- A magnetic cavity in the interstellar wind influenced by :
  - solar wind
  - solar magnetic field
- The heliospheric Termination Shock (TS) and heliosheath are the interfaces of the heliosphere with the surrounding interstellar medium
- Voyager 1,2 are currently exploring the heliosheath (between TS and heliopause)

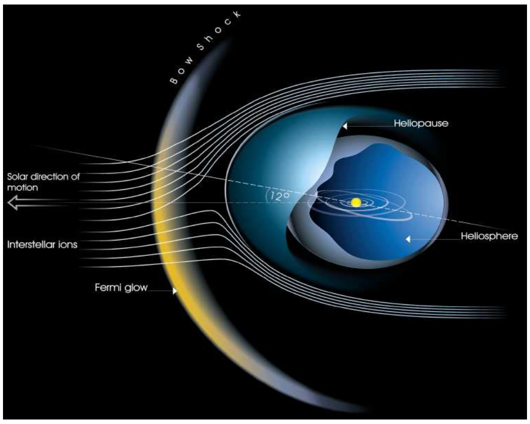

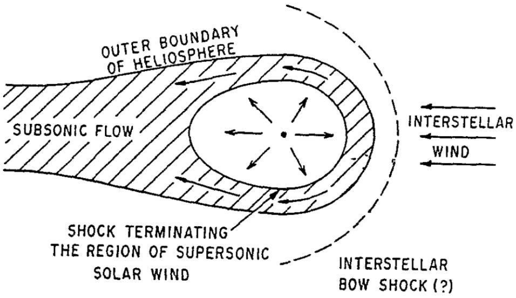

Solar wind

- ✔ A continuous flow of charged particles from SUN with velocities around 400 Km/s
  - ▶ mainly composed of electrons and protons
  - ▶ flux $\sim 10^{12}$ particles$/m^2.s$
  - ▶ first continuous observation made by Marina 2 spacecraft (1962)
  - ▶ detailed measured by the spacecraft Ulysses (three orbits)
- ✔ At solar minimum (1995) solar wind faster on poles than in equator obs (fig)
- ✔ Around 4 days to reach Earth (1 AU)
- ✔ Carries the sun magnetic field to the interplanetary space

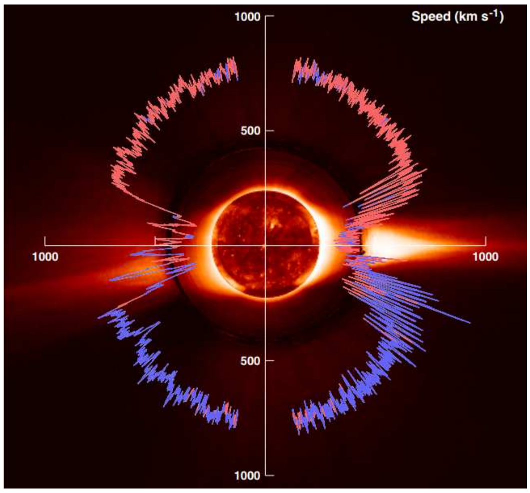

Solar magnetic field

- ✔ The SUN rotates with a period of $\simeq 27.27$ days (Carrington rotation - started on Nov 9, 1853)
- ✔ The magnetic field at the solar magnetic poles approximates that of a dipole
- ✔ Theres exist a progressive offset between the SUN magnetic and rotational axes as the SUN activity goes from minimum to maximum
  - ▶ near solar maximum the magnetic field assumes a much more complicated structure
- ✔ There exist a a reversal of the magnetic field polarity every 11 years at solar maximum
  - ▶ **polarity** $+$, field lines outward on North and inward on South

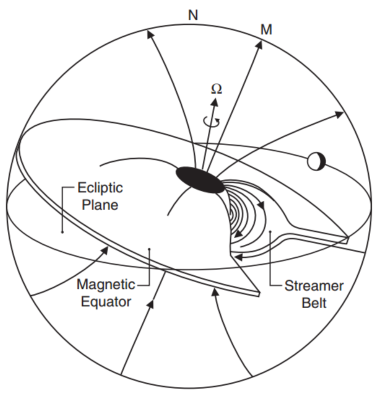

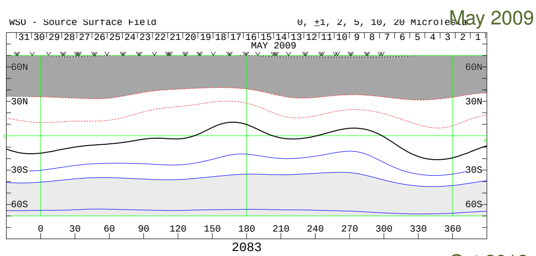

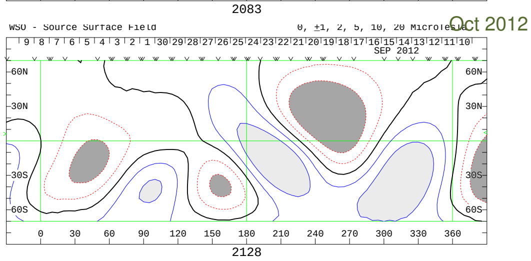

Solar activity indicators

Neutron monitors

- ✔ primary cosmic rays (protons) interact with the atmosphere and produce secondary neutrons
- ✔ the neutron component is measured by neutron monitors at different geographical altitudes and latitudes
  different geomagnetic cutoffs
- ✔ detection by proportional tubes surrounded respectively by high-Z (lead) and low-Z (polyethylene) materials to amplify secondary neutron component and shield background radioactivity

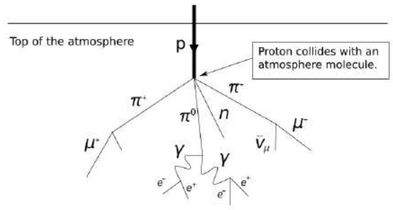

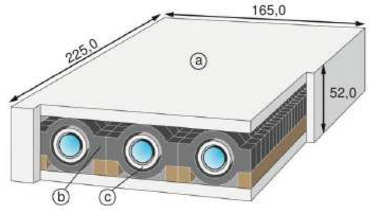

- ✔ measurement of the neutron rate provides information of CR intensity variation

Sunspots

- ✔ the number of sun dark spots (cooler than surrounding photosphere) monitors the Sun activity
  can be as large as 10^5 Km
- ✔ 11 year periodicity
- ✔ solar cycle : from a sunspot minimum to the next one (1st solar cycle : 1755-1766)

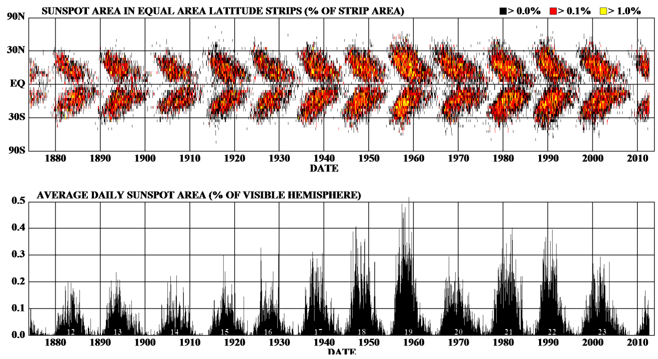

Solar cycles

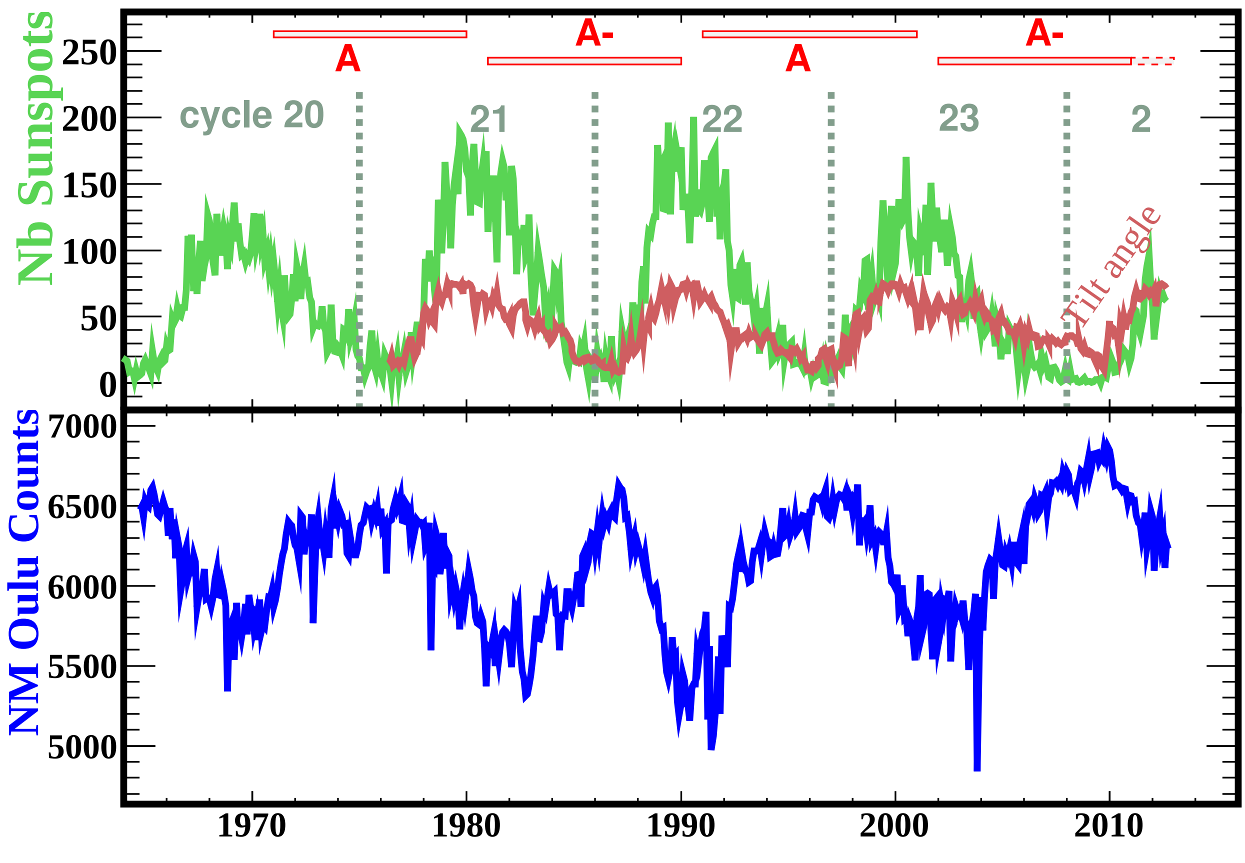

Solar flares

- ✔ A solar flare is a localized explosive release of energy that appears as a sudden, shortlived brightening of an area in the chromosphere
  - ► release of electromagnetic radiation and energetic particles
  - ► solar brilliance usually measured in optical and X-rays
- ✔ Classified according to the energy released

X-ray (1-8 Angst) index

E [ergs/$cm^2.s$]		
$C = 10^{-3}$	$M = 10^{-2}$	$X = 10^{-1}$

- ✔ Forbush decrease : cosmic rays flux present a fast decrease (March 2012, NM flux varied of $\sim 10\%$) followed by a recovering period of ~ 5 days
  - ► although more common near solar maximum, occur through all the solar cycle
- ✔ Solar flares visible on 2012 : Jan 27 (X1.7), March 7 (X5.4), July 12 (X1.4),

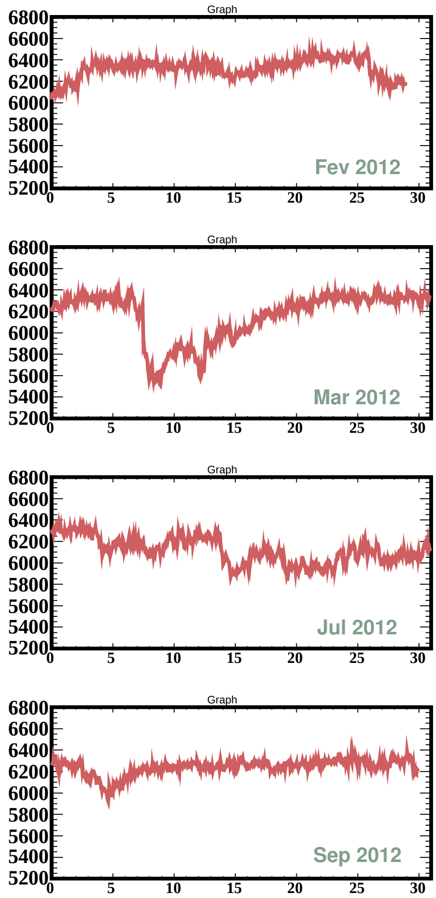

AMS02 : proton flux variability

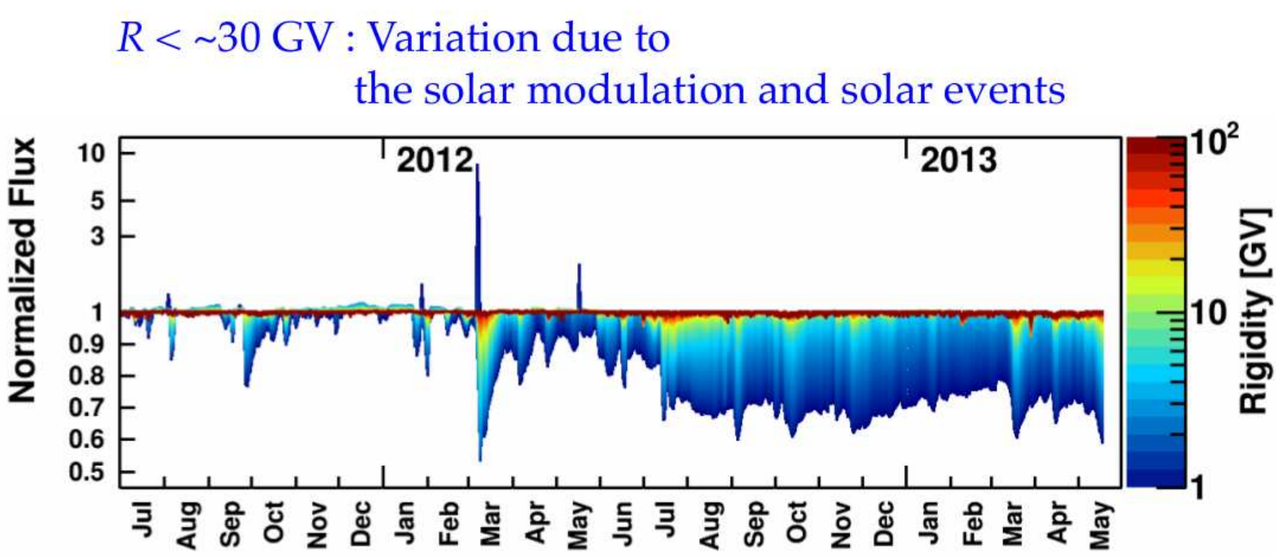

Cosmic Ray Detection

AMS detector principles

CRs detection on space

- ✔ cosmic rays (mostly protons) detection on space is feasible up to TeV's energies
  - ▶ cosmic ray flux decreases steeply with energy ($\Phi \sim E^{-2.7}$)
- ✔ a key issue on their detection is its identification ($\gamma, p, \bar{p}, e^{\pm}, he, \ldots$)
- ✔ a detector on space capabilities :
  - ▶ fast trigger events (event rate depends on geomagnetic detector position)
  - ▶ electric charge
  - ▶ velocity
  - ▶ rigidity ($Rig = \frac{pc}{Ze}$) and energy
- ✔ carried by satellites (ISS) or balloons
  - ▶ Explorer-I (1958) carried the 1st CR detector (Geiger counter)
  - ▶ Van Allen belts discovered

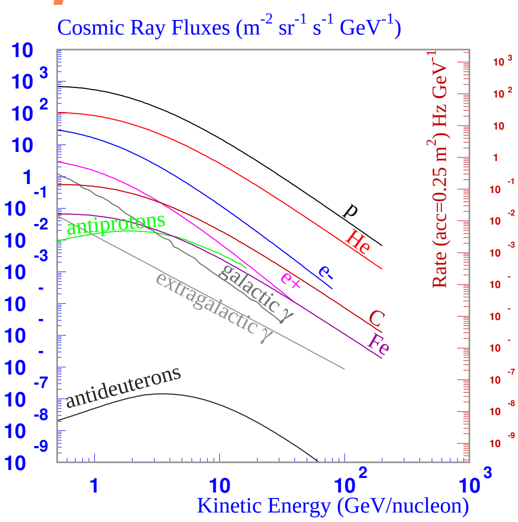

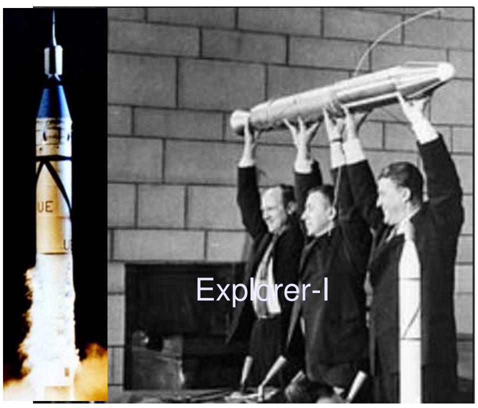

AMS on ISS : a long journey...

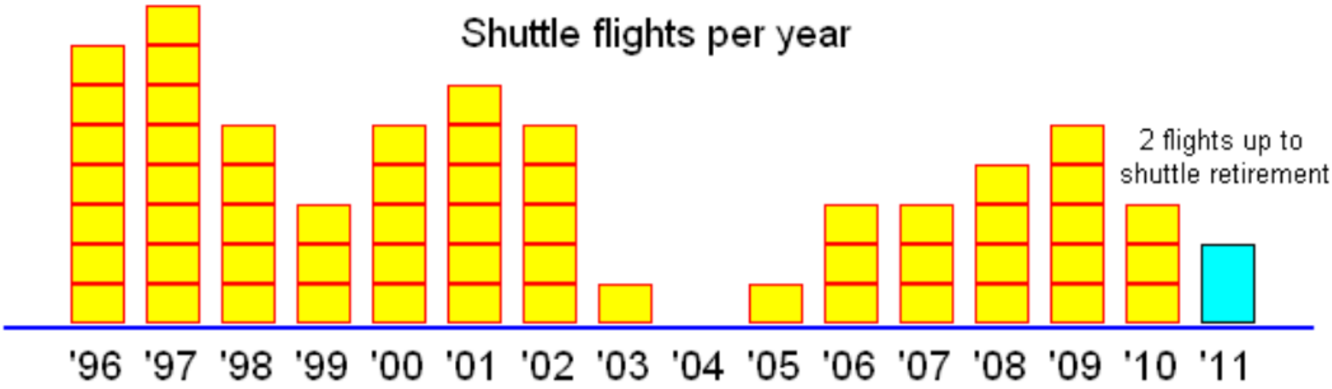

STS-91 flight (Jun 98)

BESS-POLAR (2004, 2007-08)

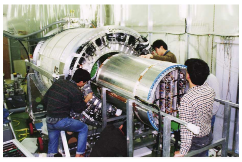

FERMI (June 2008)

PAMELA (June 2006)

AMS to ISS (16-19 May 2011)

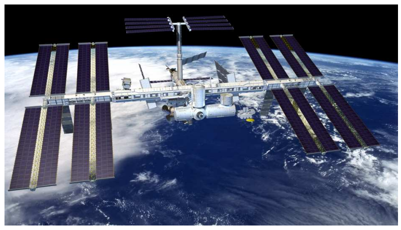

AMS02 detector

- ✔ detector installed on the International Space Station the 19 May 2011
- ✔ orbiting around earth at around 400 Km of altitude
  orbit ~ 90 min long
- ✔ around 40 million events gathered/day
  ~ 100 GBytes to transfer every day at 10 Mb/s through relay satellites (TDRS)
- ✔ $16\ 10^9$ triggers/year
  35 TBytes of raw data
- ✔ 36 billions of events collected till now (Jul 2013)

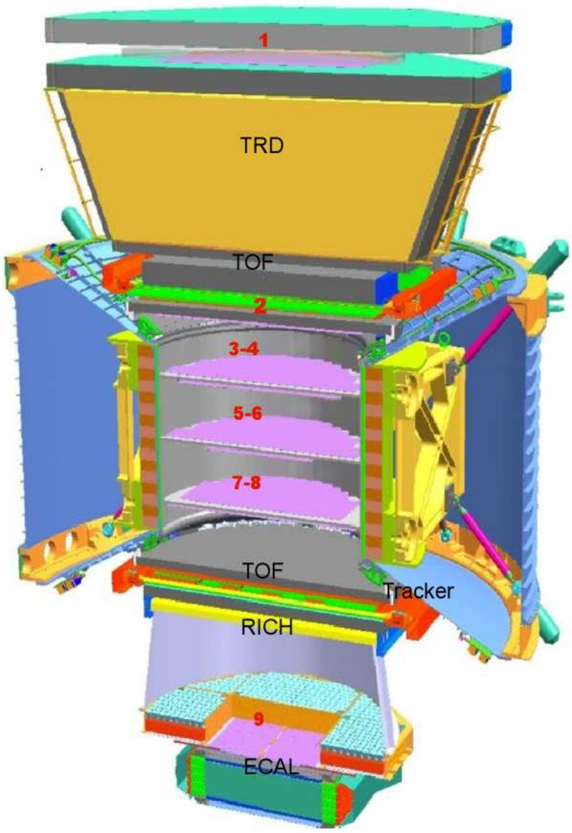

AMS02 on ISS

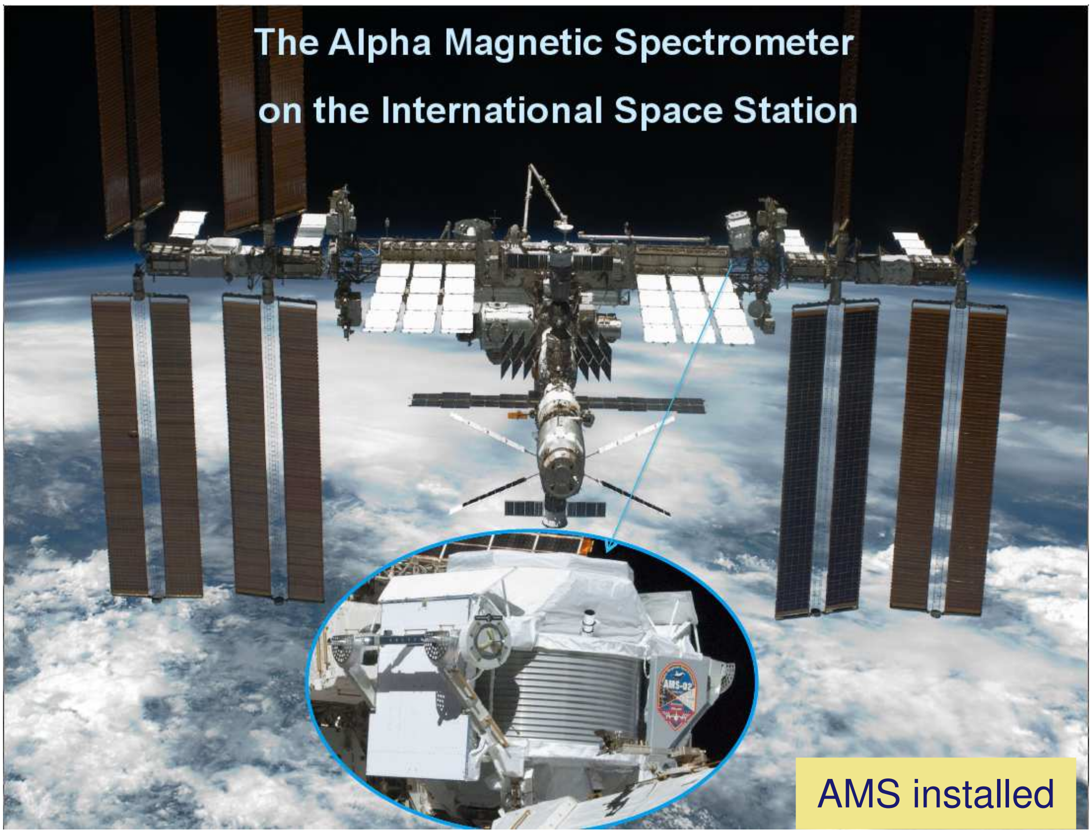

Time-of-Flight (TOF)

- ✔ 4 scintillator planes (around $1.4\ m^2$)
- ✔ a total of 34 paddles/counters large of 12 cm and overlaying 0.5 cm

plane	counters	PMTs
1	8	36
2	8	32
3	10	40
4	8	36

- ✔ light guides twisted/bended to minimize magnetic field effects
- ✔ $2/3$ PMT's for light readout at both ends

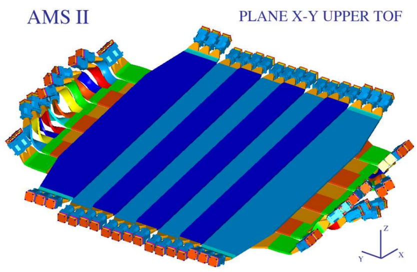

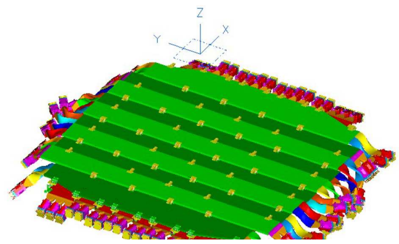

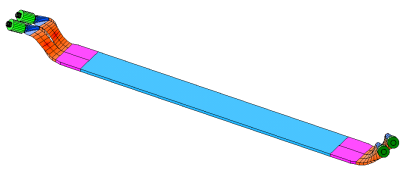

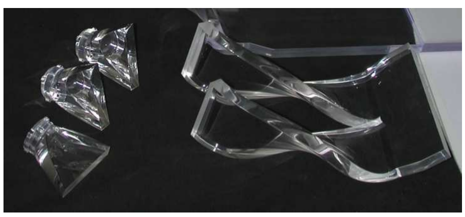

Time-of-Flight (TOF)

- ✔ 4 scintillator planes (around $1.4\ m^2$)
- ✔ a total of 34 paddles/counters large of 12 cm and overlaying 0.5 cm

plane	counters	PMTs
1	8	36
2	8	32
3	10	40
4	8	36

- ✔ light guides twisted/bended to minimize magnetic field effects
- ✔ $2/3$ PMT's for light readout at both ends

- ✔ fast trigger (3×4) on $200\ nsec$
- ✔ velocity $(\vec{v})$ and charge (z)
- ✔ upward/dowward particle separation (10^{-9})

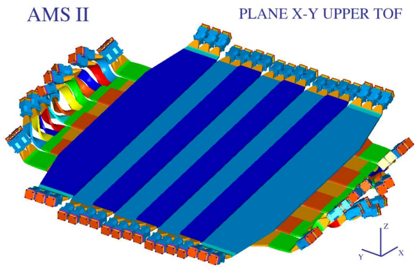

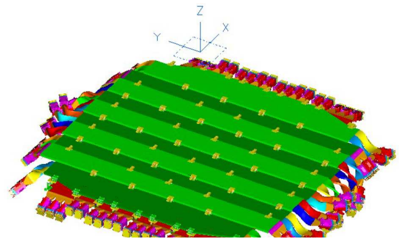

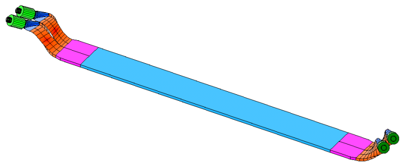

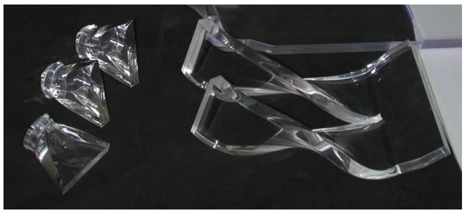

Scintillators properties

Material	eV/photon	τ [nsec]	λ_{max} [nm]	ρ [g/cm^3]	$\frac{dE}{dx}$ (mip) [MeV/cm]	n	Notes
Anthracene	60 (100%)	30	447	1.25		1.62	
Plastic NE104	88 (68%)	1.9	406	1.032	~ 2	1.58	
NaI	26 (230%)	230	413	3.67	4.8	1.85	Hygro
CsI(Na)	90 (150%)	650	420	4.51	~ 5	1.79	
BGO	173	300	480	7.13	9.2	2.20	

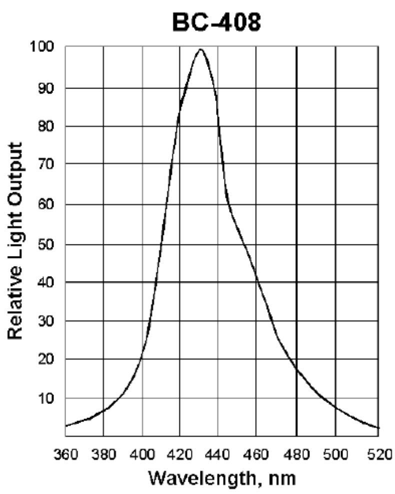

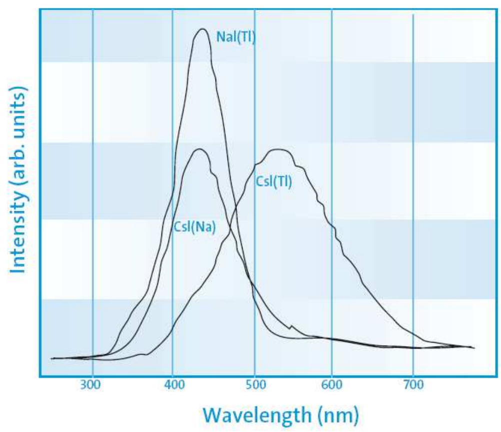

Velocity measurement (β) with TOF

✔ particle velocity is derived from measuring the time difference (Δt) between the upper and lower scintillator planes and the track length (Δs)

$$\boxed{\beta = \frac{\Delta s}{c\Delta t}} \qquad \boxed{\frac{\sigma\beta}{\beta} = \frac{\beta c}{\Delta s}\sigma_t}$$

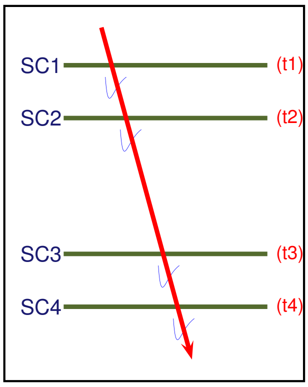

Velocity measurement (β) with TOF

✔ particle velocity is derived from measuring the time difference (Δt) between the upper and lower scintillator planes and the track length (Δs)

$$\boxed{\beta = \frac{\Delta s}{c\Delta t}} \qquad \boxed{\frac{\sigma\beta}{\beta} = \frac{\beta c}{\Delta s}\sigma_t}$$

✔ single pad error (σ_t) depends on :

- signal shape $(\sigma_1/\sqrt{N})$
- photons path length dispersion $(\sigma_2\ d/\sqrt{N})$
- electronic noise (σ_3)

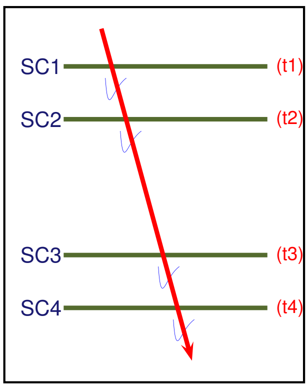

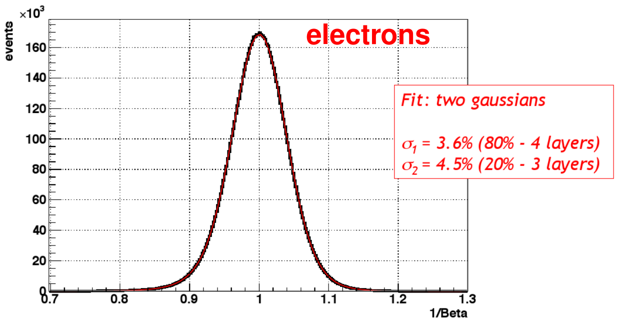

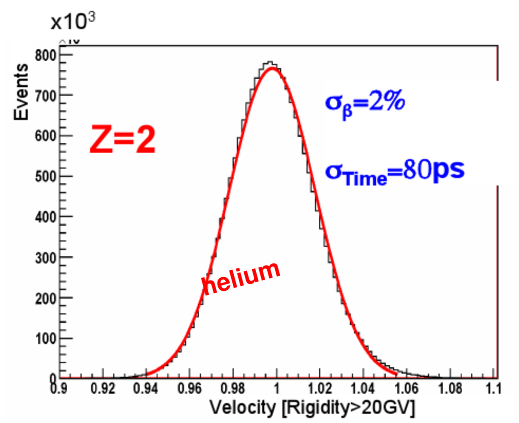

Charge measurement (Z) with TOF

- ✔ energy deposited on scintillator $\Delta E \propto Z^2$
- ✔ up to 4 ΔE samplings
- ✔ dominant uncertainty comes from energy deposition fluctuations

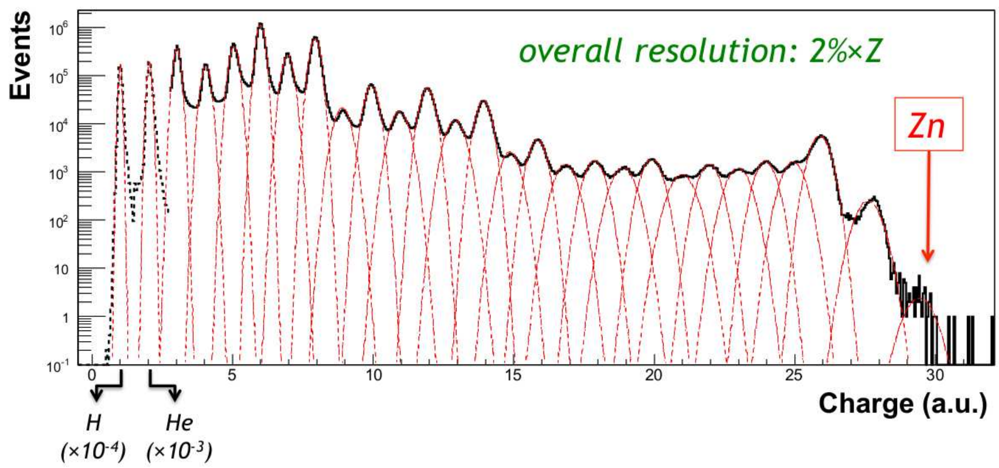

Magnetic field : permanent magnet

Nd-Fe-B magnet
0.15 T in the magnet center
No leak out (B_{out}<0.02T) to avoid torque on structures

120k locations 3D map.
Deviation from 1997 (AMS-01) < 1%

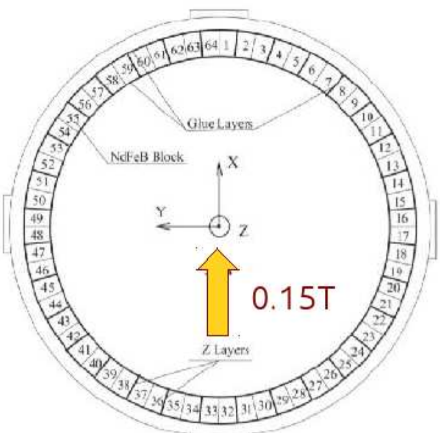

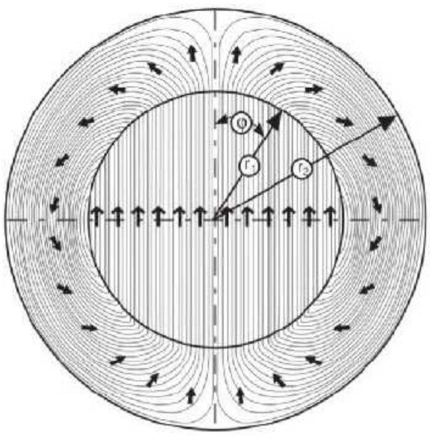

Silicon Tracker

- ✔ 6 *planes* instrumented with silicon sensors (3 inside the magnet and 3 outside)
- ✔ 9 *layers* of double-sided silicon microstrip sensors
- ✔ ~ 2500 *sensors* arranged on 192 *ladders*
  $7-15$ sensors per ladder with a size of $28-60$ cm
- ✔ readout pitch
  $110\mu m$ along bending direction y
  ($208\mu m$) along non-bending direction x

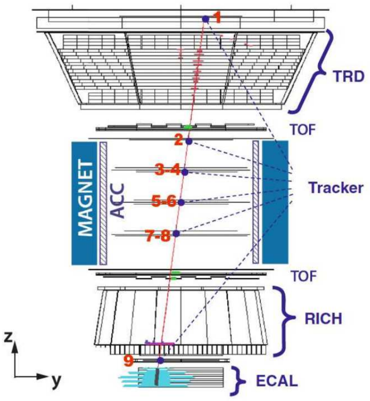

- ✔ 9 independent position measurements of the particle track
- ✔ particle rigidity ($P \equiv \frac{pc}{Ze}$) from track reconstruction
- ✔ electric charge (Z) from energy deposition (dE/dx)

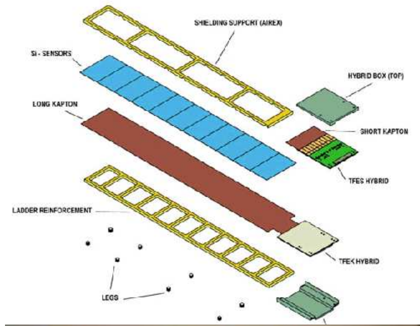

Rigidity measurement

- ✔ charged particles bend under magnetic field ($B \sim 0.15$ T)
- ✔ 9 silicon double-sided layers crossed
- ✔ *spatial resolution*
  $10\ \mu m$ on bending plane (y)
  $30\ \mu m$ on non-bending plane (x)
- ✔ trajectory bending (sagitta) is measured : $s \propto \frac{L \int B d\ell}{P}$
- ✔ rigidity ($P = pc/Ze$) resolution
  $\sim 10\%$ at 10 GV and MDR $\sim\ 2$ TV for protons
  degradation at low rigidities due to Multiple Scattering

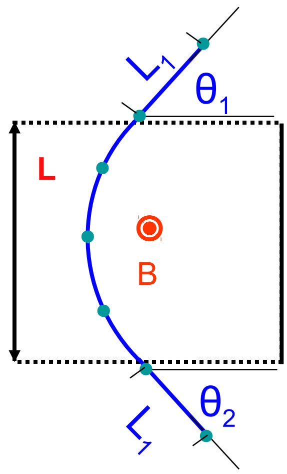

Rigidity measurement

- charged particles bend under magnetic field ($B \sim 0.15$ T)
- 9 silicon double-sided layers crossed
- *spatial resolution*
  $10\ \mu m$ on bending plane (y)
  $30\ \mu m$ on non-bending plane (x)
- trajectory bending (sagitta) is measured : $s \propto \frac{L \int B d\ell}{P}$
- rigidity ($P = pc/Ze$) resolution
  $\sim 10\%$ at 10 GV and MDR $\sim\ 2$ TV for protons
  degradation at low rigidities due to Multiple Scattering

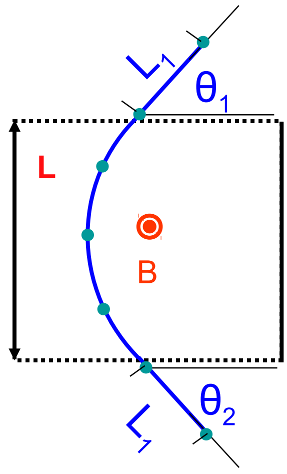

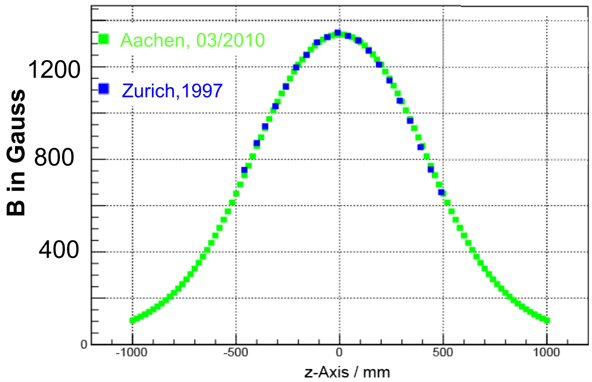

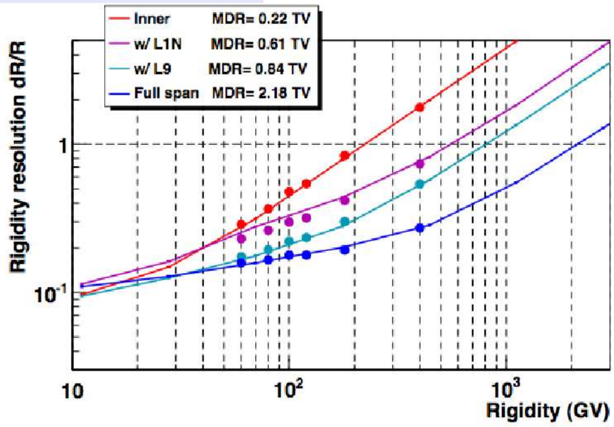

energy deposition : $dEdx$

The energy deposition on TOF layers together with the rigidity ($P = pc/Ze$) measurement is sensitive to A/Z : 1 for protons, 2 for light nuclei

$$\beta = \frac{E}{pc} = \frac{\sqrt{(pc)^2 + (Mc^2)^2}}{pc} = \sqrt{1 + \left(\frac{A}{Z}\right)^2 \left(\frac{m_0}{P}\right)^2}$$

energy deposition : $dEdx$

The energy deposition on TOF layers together with the rigidity ($P = pc/Ze$) measurement is sensitive to A/Z : 1 for protons, 2 for light nuclei

$$\beta = \frac{E}{pc} = \frac{\sqrt{(pc)^2 + (Mc^2)^2}}{pc} = \sqrt{1 + \left(\frac{A}{Z}\right)^2 \left(\frac{m_0}{P}\right)^2}$$

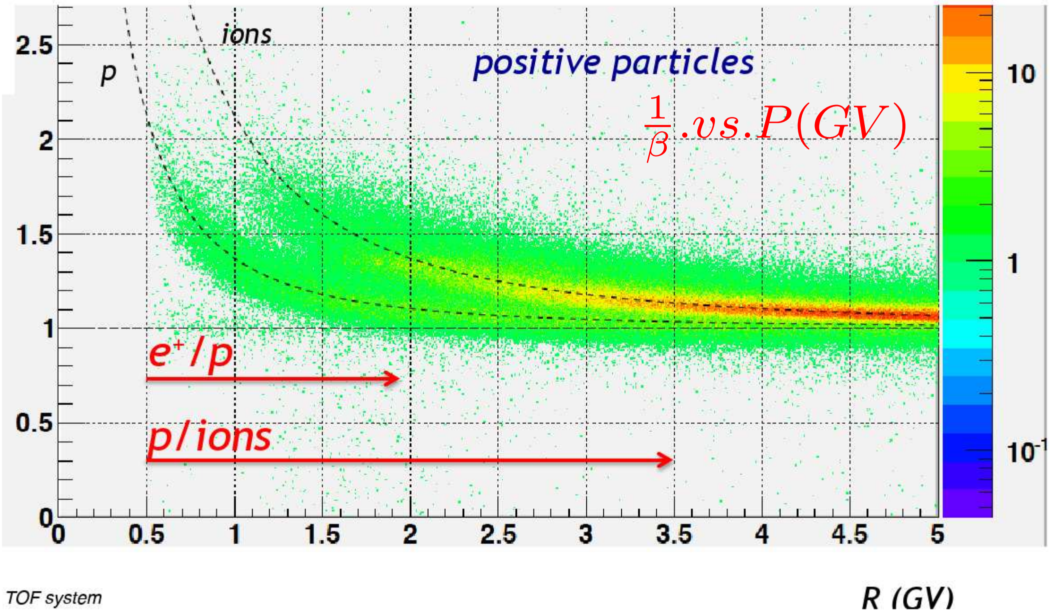

Charge measurement (Z) with Tracker

- ✔ energy deposited on silicon sensors ($300\ \mu$m) : $\Delta E \propto Z^2$
- ✔ up to 9 ΔE samplings

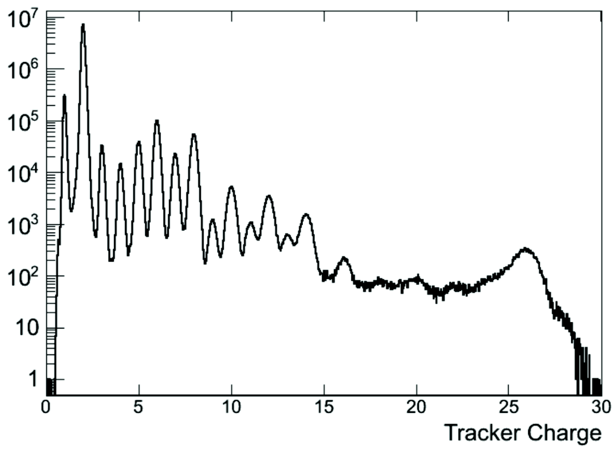

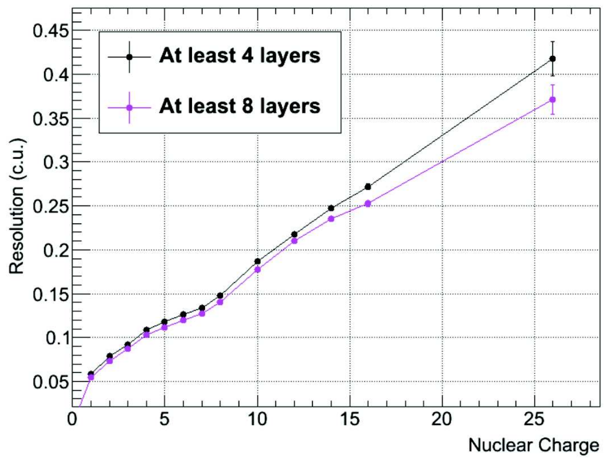

Transition radiation : principles

- ✔ Electromagnetic radiation is emitted when a charged particle traverses a medium with a varying dielectric permitivity (ε)
- ✔ A transition radiator will consist on a series of foils and air gaps
  - ▶ polyethilene foam
  - ▶ fleece
- ✔ X-rays are emitted
- ✔ To avoid X-ray absorption in radiator foils, its atomic number Z has to be as low as possible
- ✔ The X-rays are detected by proportional tubes filled with a mixture of Xe/CO_2 (80%/20%)

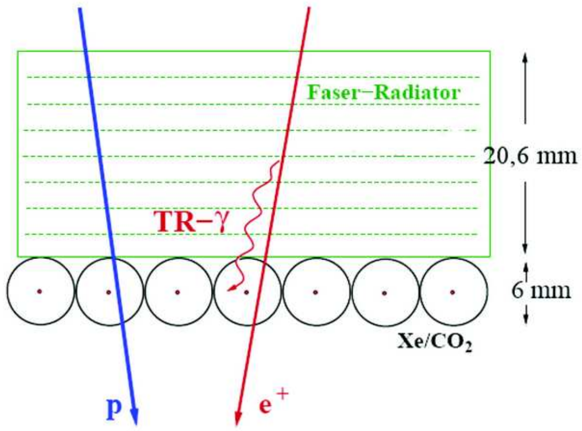

Transition Radiation Detector (TRD)

- ✔ *modules (328) made of fleece radiator and straw tubes*
  - ▶ 16 straw tubes per module
  - ▶ radiator thickness of $23\ mm$
  - ▶ straw tubes ($\Phi = 6\ mm$) filled with Xe/CO_2
- ✔ 20 *layers* assembled on a octogonal shape
  - ▶ 4 layers on upper/lower part along the bending plane
  - ▶ 12 layers on the middle transversally placed

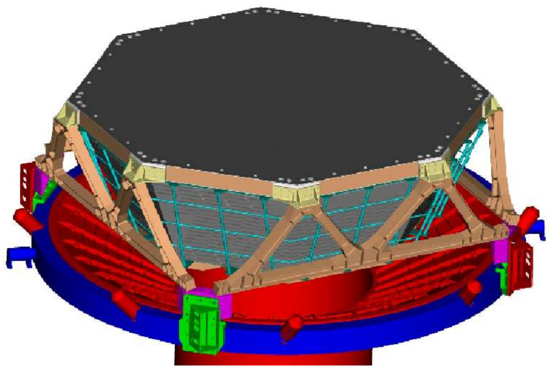

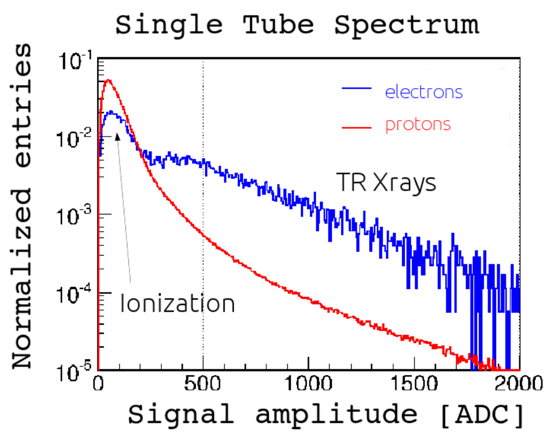

- ✔ evaluation of the particle $\gamma = \frac{E}{m}$ boost
- ✔ separation of particles with extreme mass differences

Charge measurement with TRD

- ✔ define PDFs for every charge and determine probability

$$P(Z) = \prod_{i}^{Nhits} PDF_i(Z)$$

- ✔ charge determined from weighted mean of two most likely charges

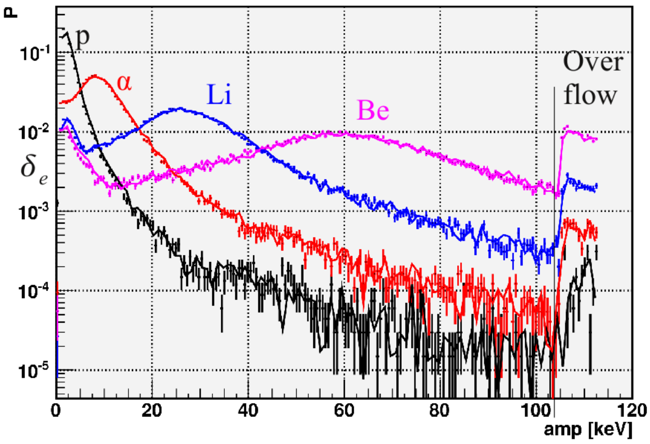

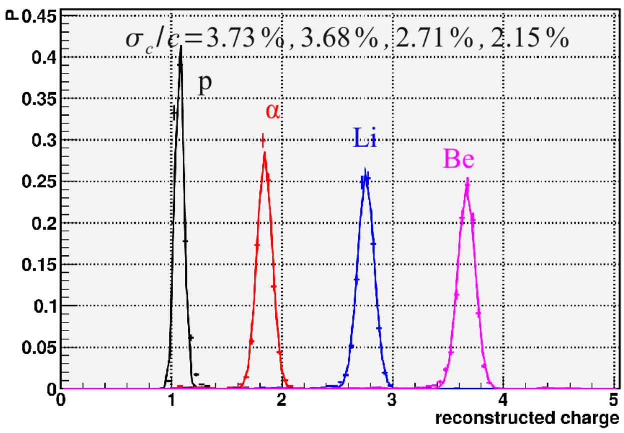

Ring Imaging Cerenkov Detector (RICH)

Construction

- ✔ proximity focusing Ring Imaging Detector
- ✔ dual solid radiator configuration
  low index aerogel : $n = 1.050$, $2.5\ cm$ thickness
  sodium fluoride : $n = 1.334$, $0.5\ cm$ thickness
- ✔ conical reflector 85% reflectivity
- ✔ photomultiplier matrix
  680 multipixelized (4×4) detectors
- ✔ spatial pixel granularity : $8.5 \times 8.5\ mm^2$

It provides

- ✔ accurate particle velocity measurement
  $\Delta\beta/\beta \sim 0.1\%$ for protons
- ✔ electric charge determination
  $\Delta Z \sim 0.2$
- ✔ albedo rejection
  directional sensitivity

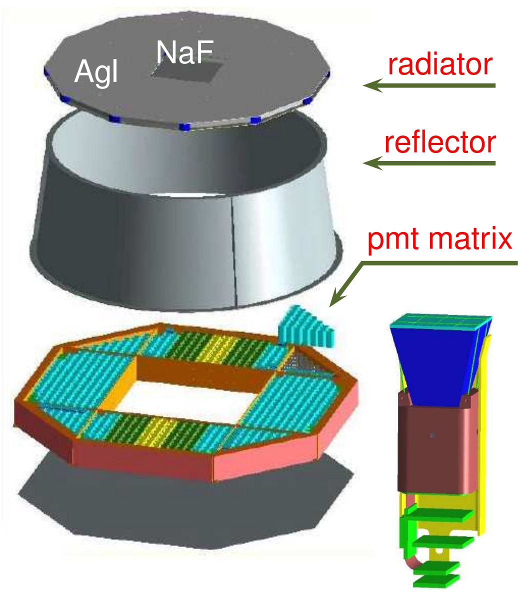

Ring Imaging Cerenkov Detector (RICH)

Construction

- ✔ proximity focusing Ring Imaging Detector
- ✔ dual solid radiator configuration
  low index aerogel : $n = 1.050$, $2.5\ cm$ thickness
  sodium fluoride : $n = 1.334$, $0.5\ cm$ thickness
- ✔ conical reflector 85% reflectivity
- ✔ photomultiplier matrix
  680 multipixelized (4×4) detectors
- ✔ spatial pixel granularity : $8.5 \times 8.5\ mm^2$

It provides

- ✔ accurate particle velocity measurement
  $\Delta\beta/\beta \sim 0.1\%$ for protons
- ✔ electric charge determination
  $\Delta Z \sim 0.2$
- ✔ albedo rejection
  directional sensitivity

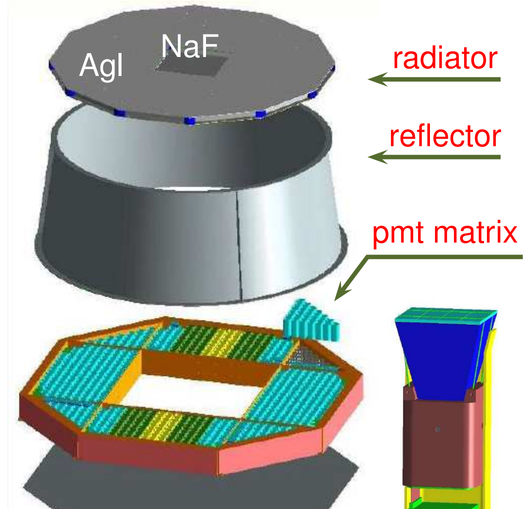

Velocity measurement with the RICH

- ✔ The AMS Tracker provides the **particle direction** (θ, ϕ) and **impact point** at the RICH radiator
- ✔ **Ring of cerenkov photons** is function of θ_c
  geometrical and likelihood methods applied to reconstruct θ_c
- ✔ Velocity obtained from θ_c measurement
  $\boxed{\beta = 1/n\ \cos\theta_c}$

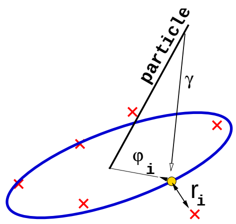

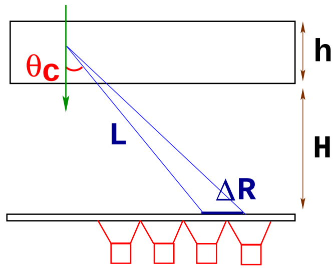

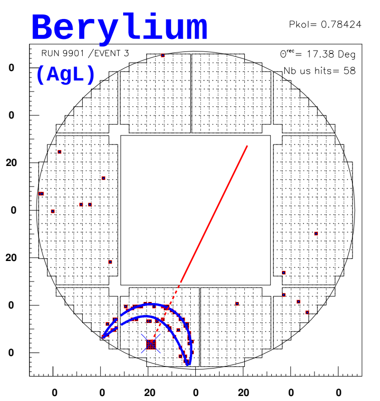

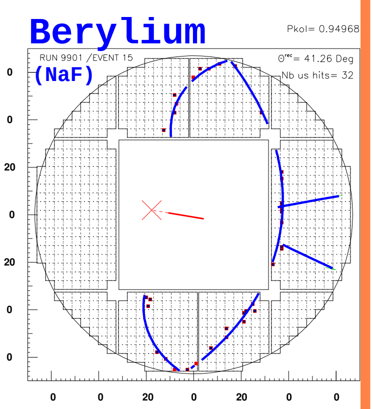

Velocity measurement with the RICH

- ✔ The AMS Tracker provides the **particle direction** (θ, ϕ) and **impact point** at the RICH radiator
- ✔ **Ring of cerenkov photons** is function of θ_c
  geometrical and likelihood methods applied to reconstruct θ_c

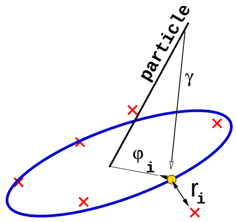

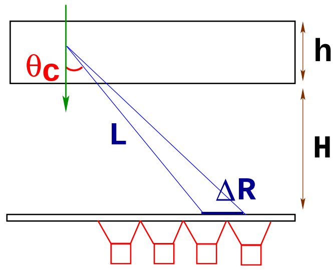

- ✔ Velocity obtained from θ_c measurement
  $\boxed{\beta = 1/n\ \cos\theta_c}$
- ✔ sources of β uncertainties :
  - ▶ pixel size (8.5 mm)
  - ▶ radiator chromaticity, $n(\lambda)$
  - ▶ radiator thickness $(h \tan\theta_c)$
    photon emission point unknown

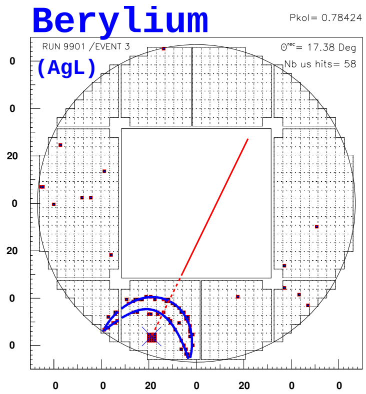

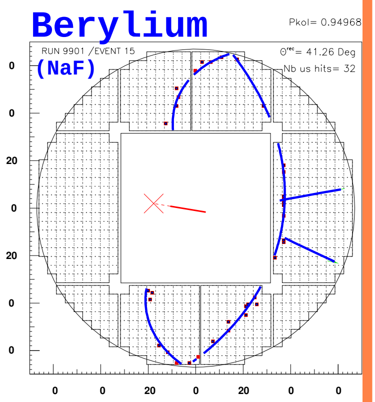

$$\boxed{\frac{\Delta\beta}{\beta} = \tan\theta_c \frac{\Delta\theta_c}{\sqrt{N_{pe}}}}$$

$$\boxed{\Delta\theta_c = (\Delta\theta_c)^{pixel} \oplus (\Delta\theta_c)^{thick} \oplus (\Delta\theta_c)^{chrom}}$$

$\boxed{\Delta\theta_c^{(i)} \simeq \frac{\Delta R_i}{H} \cos^2\theta_c}$ i=pixel,thickness

$\boxed{\Delta\theta_c^{(i)} \simeq \frac{1}{\tan\theta_c} \frac{\Delta n}{n}}$ i=chromat.

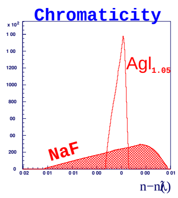

	$\Delta\theta_c^{geom}$ (mrad)		$\Delta\theta_c^{chrom}$	$\boldsymbol{\Delta\theta_c}$	$(\boldsymbol{\Delta}\beta/\beta)_{\mathbf{hit}}$
	$\Delta\theta_c^{thick}$	$\Delta\theta_c^{pixel}$	(mrad)	(mrad)	$(\beta \simeq 1)$
AGL	3.3	4.6	3.2	6.5	$\mathbf{2.1\ 10^{-3}}$
NaF	0.3	0.6	4.8	4.8	$\mathbf{4.2\ 10^{-3}}$

Light yield and RICH velocity

The different radiator indexes (agl, naf) imply different light yields and velocity resolutions

the more photons we have the best is the accuracy of the measurement ❒ number of p.e. for fully contained rings and vertical incidence

N'_N, number of photoelectrons for fully contained rings and particle inciding vertically in the detector

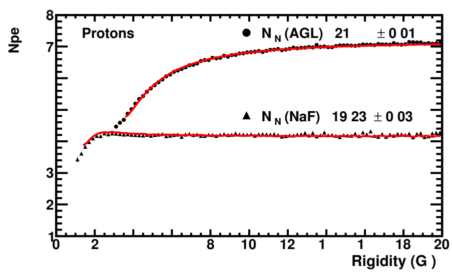

Light yield and RICH velocity

The different radiator indexes (agl, naf) imply different light yields and velocity resolutions

the more photons we have the best is the accuracy of the measurement ❐ number of p.e. for fully contained rings and verti

N'_N, number of photoelectrons for fully contained rings and particle inciding vertically in the detector

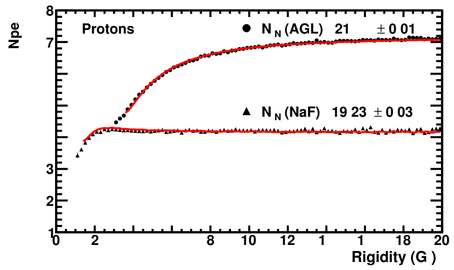

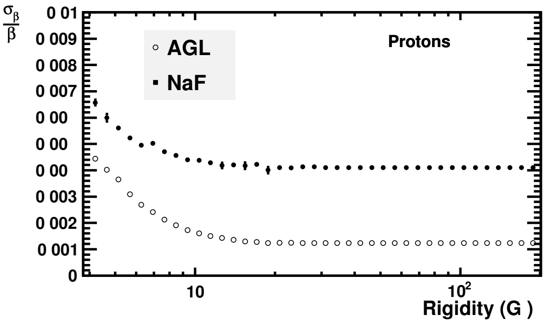

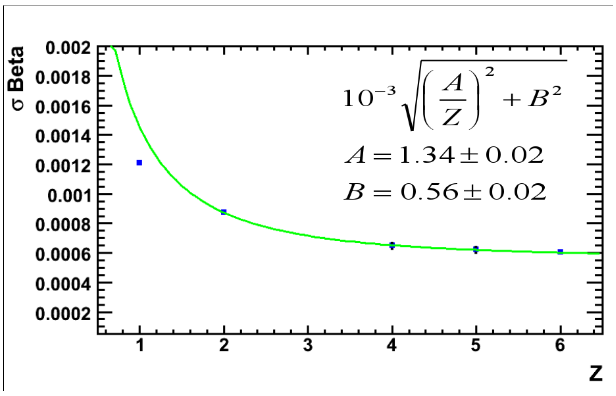

Charge determination with the RICH

✔ Charge determination :

$$\boxed{Z^2 \propto \frac{N_{p.e}}{\varepsilon}}$$

$\varepsilon \equiv$ ring efficiency

ring acceptance, γ absorption,...

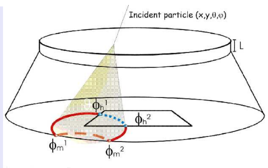

✔ Z Uncertainties :

- ▶ statistical : $\Delta N_{p.e} = \sqrt{N_{p.e}\left(1+\sigma^2_{p.e}\right)}$
- ▶ systematics from non-uniformities :
  - radiator : n, thickness, clarity, ...
  - detection : LG, PMT, temperature effects, ...

$$\boxed{\Delta Z = \frac{1}{2}\sqrt{\frac{1+\sigma^2_{p.e}}{N_0} + Z^2\left(\frac{\Delta\varepsilon}{\varepsilon}\right)^2}}$$

✔ results from test beam (2003) with fragmented ions and ISS data

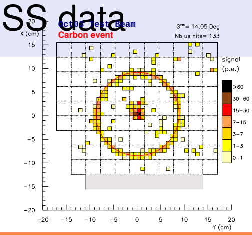

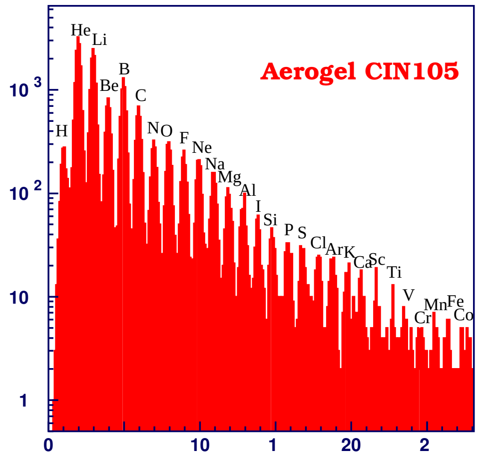

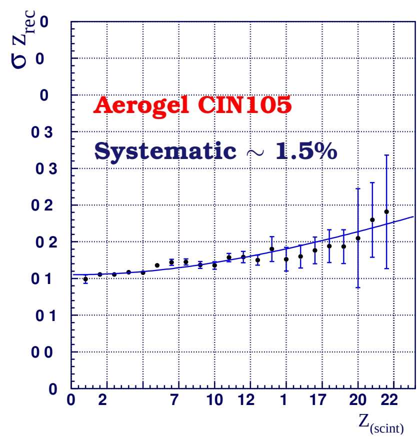

Charge determination with the RICH

- ✔ Charge determination :

  $\boxed{Z^2 \propto \frac{N_{p.e}}{\varepsilon}}$

  $\varepsilon \equiv$ ring efficiency

  ring acceptance, γ absorption,...

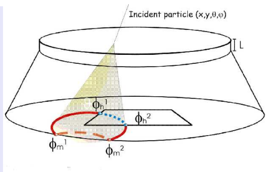

- ✔ Z Uncertainties :
  - ▶ statistical : $\Delta N_{p.e} = \sqrt{N_{p.e}\left(1+\sigma^2_{p.e}\right)}$
  - ▶ systematics from non-uniformities :
    - ● radiator : n, thickness, clarity, ...
    - ● detection : LG, PMT, temperature effects, ...

  $$\boxed{\Delta Z = \frac{1}{2}\sqrt{\frac{1+\sigma^2_{p.e}}{N_0} + Z^2\left(\frac{\Delta\varepsilon}{\varepsilon}\right)^2}}$$

- ✔ results from test beam (2003) with fragmented ions and ISS data

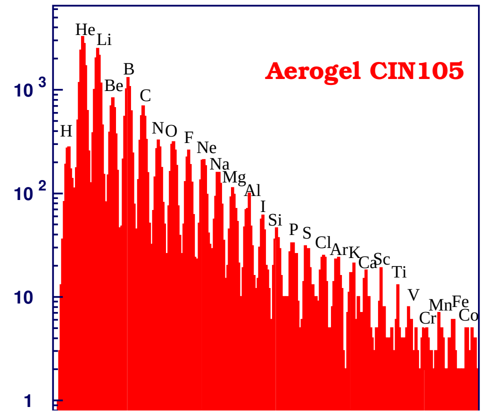

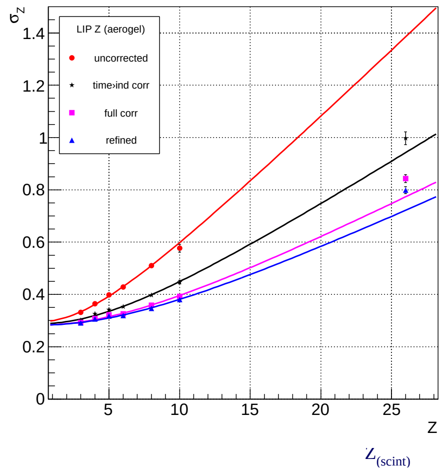

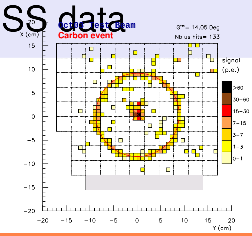

Electromagnetic Calorimeter (ECAL)

- ✔ sampling e.m. calorimeter with lead+scintillating fibers structure

  $648 \times 648 \times 167\ mm^3$

  lead (58%), fibers (33%), optical glue (9%)

  $\rho \sim 6.8\ gr/cm^3$
- ✔ 9 superlayers disposed along X and Y alternately

  $4(5)$ disposed along the X (Y)
- ✔ $\sim 17X_0(\sim 1cm)$ radiation lengths
- ✔ multi-pixel (2×2) photomultiplier's

  large dynamic range
- ✔ 18 samplings of e.m shower

  cell granularity $\sim 0.5\ R_M$ (35 fibers per PM pixel)
- ✔ detector acceptance : $0.06\ m^2.sr$

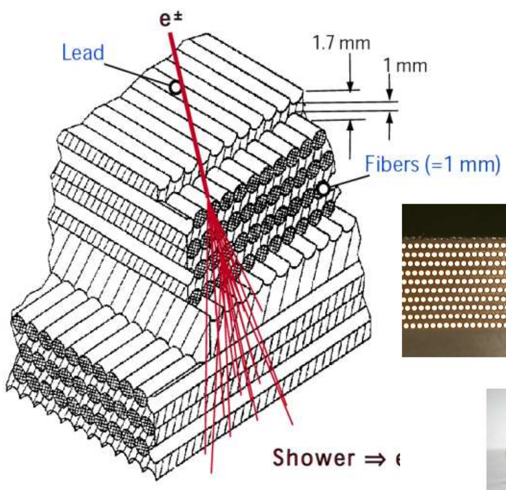

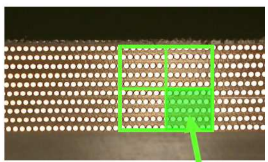

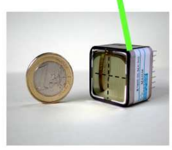

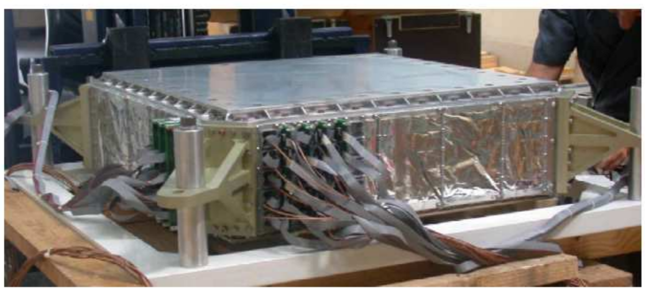

- ❒ $e^{\pm}, \gamma$ energy measurement
- ❒ particle direction
- ❒ fast trigger signal (dynode)

ECAL : energy measurement

- ✔ electrons (positrons) and photons interact with the material creating an electromagnetic shower composed of $e^{\pm}, \gamma$
- ✔ shower maximum is reached when shower particles stop replication (through bremmssthralung and pair-production mechanisms) and start to be absorbed
- ✔ the transverse dimension of the shower is determined by the low energy multiple scattering
  molière radius : $R_M = \frac{21}{E_c/MeV} X_0 \sim 2\ cm$
- ✔ the shower is sampled longitudinally several times
  active medium (scintillating fibers) measures the shower deposited signal
- ✔ energy resolution : statistical uncertainty
  $\frac{\Delta E}{E} = \frac{\sqrt{N}}{N} = \frac{1}{\sqrt{N}} \propto \frac{1}{\sqrt{E}}$

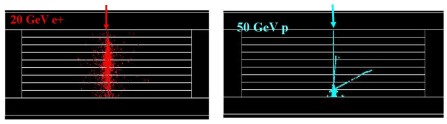

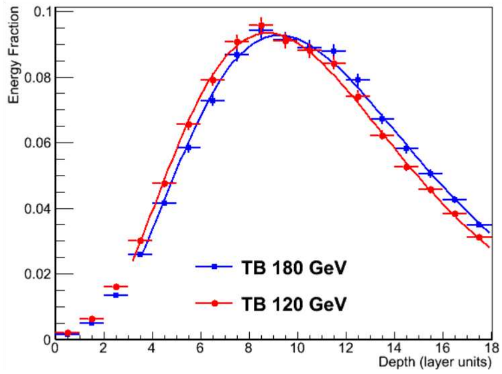

ECAL : energy measurement

- ✔ electrons (positrons) and photons interact with the material creating an electromagnetic shower composed of $e^{\pm}, \gamma$
- ✔ shower maximum is reached when shower particles stop replication (through bremmssthralung and pair-production mechanisms) and start to be absorbed
- ✔ the transverse dimension of the shower is determined by the low energy multiple scattering
  molière radius : $R_M = \frac{21}{E_c/MeV} X_0 \sim 2\ cm$
- ✔ the shower is sampled longitudinally several times
  active medium (scintillating fibers) measures the shower deposited signal
- ✔ energy resolution : statistical uncertainty
  $\frac{\Delta E}{E} = \frac{\sqrt{N}}{N} = \frac{1}{\sqrt{N}} \propto \frac{1}{\sqrt{E}}$

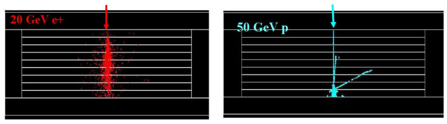

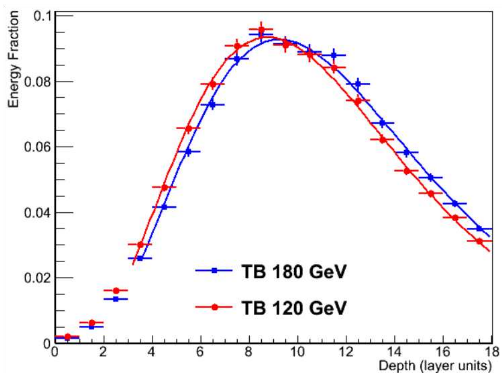

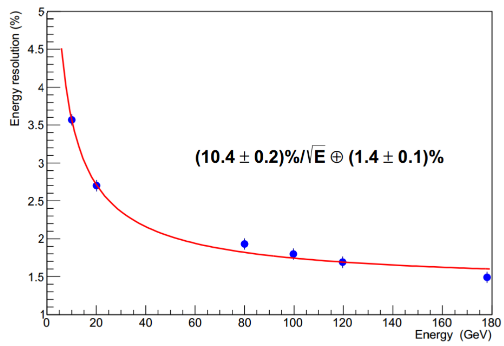

AMS02
positron ratio

analysis and results

Positron analysis

- ✔ positron analysis has to deal with a large background from protons (and also electrons, but here charge sign helps !)
  $\frac{\Phi_p}{\Phi_e^+} \sim 10^3 - 10^4$
- ✔ AMS detector requirements : good positron identification and capability of strongly reject protons
  ECAL, TRD, TRACKER
  at low energy TOF and RICH also contribute

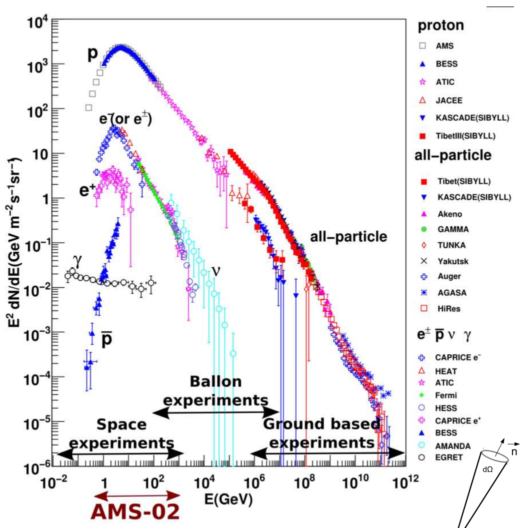

background rejection factor, R_f
The rejection factor measures the capability to suppress the background channel

$$\frac{N_S}{N_B} = \frac{\Phi_S}{\Phi_B}\,\frac{G\ \varepsilon_0\ \varepsilon_S^c}{G\ \varepsilon_0\ \varepsilon_B^c} = \frac{\Phi_S}{\Phi_B}\,\underbrace{\frac{\varepsilon_S^c}{\varepsilon_B^c}}_{R_f} = \frac{\Phi_S}{\Phi_B/R_j}$$

G = geometrical acceptance
ε_0 = general selection
ε_i^c = specific selection

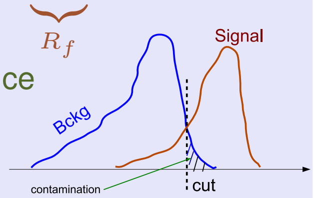

acceptance, G
$G = \int_{A,\Omega} d\Omega \vec{n} \cdot d\vec{A} \quad [m^2.sr]$

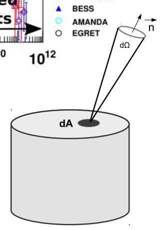

signal purity, S_p
it measures the purity of the signal for a specific (c) selection

$$S_p = \frac{N_S^c}{N_S^c + N_B^c}$$

Positron identification with TRD

the electron and proton track signal is sampled up to 20 times in TRD

$$\boxed{P_{e,p} = \sqrt[n]{\Pi_{i=1}^{n} \, p_i^{e,p}}} \quad \Rightarrow \quad \boxed{L_e = -\ln\left(\frac{P_e}{P_e+P_p}\right)}$$

$p_i^{e,p}$: layer probability of an electron or proton signal deposition

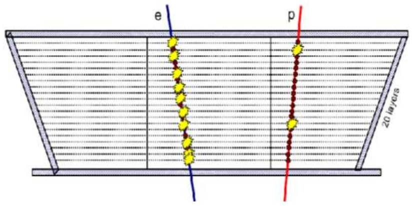

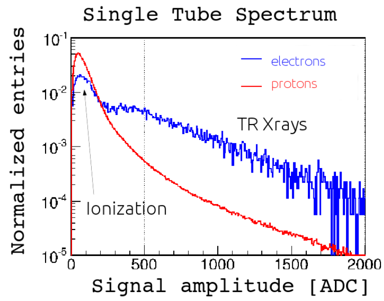

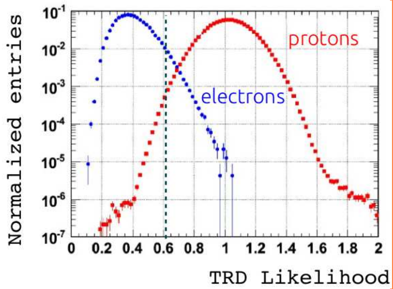

TRD estimator : $L_{e,p}$

Positron identification with TRD

the electron and proton track signal is sampled up to 20 times in TRD

$$\boxed{P_{e,p} = \sqrt[n]{\Pi_{i=1}^{n} \, p_i^{e,p}}} \quad \Rightarrow \quad \boxed{L_e = -\ln\left(\frac{P_e}{P_e+P_p}\right)}$$

$p_i^{e,p}$: layer probability of an electron or proton signal deposition

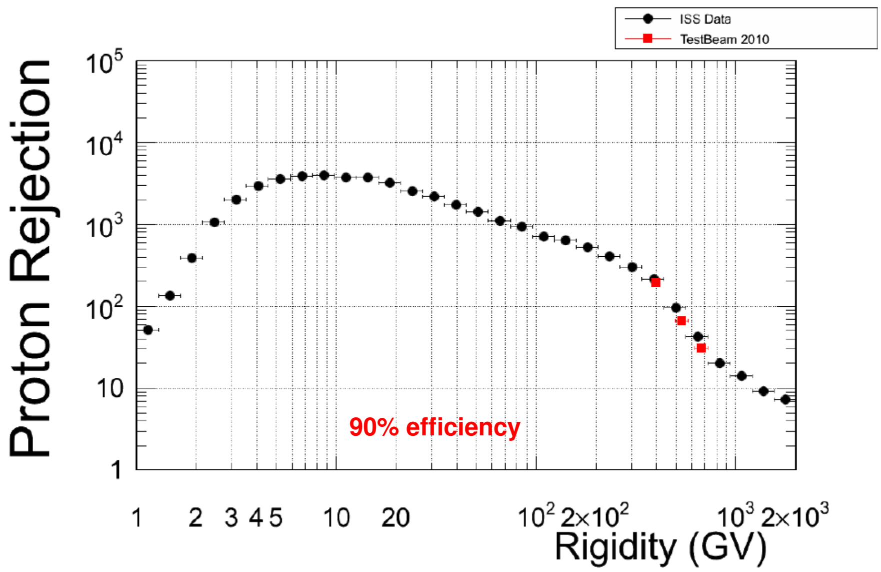

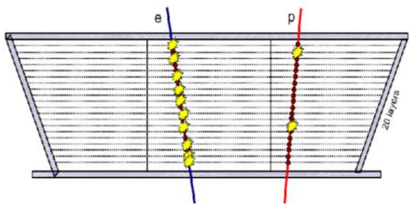

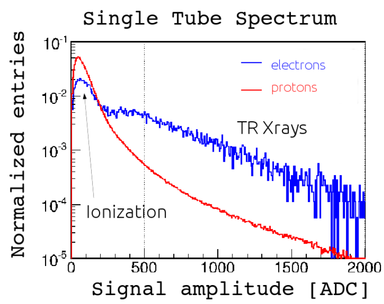

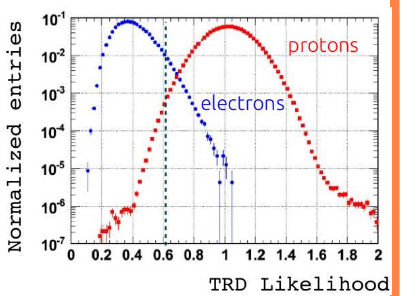

TRD estimator : $L_{e,p}$

Positron identification with ECAL

electron and proton create different "tracks" in electromagnetic calorimeter (ECAL)

Boost Decision Tree (BDT) folds the different observables that can distinguish both particles, into one cut

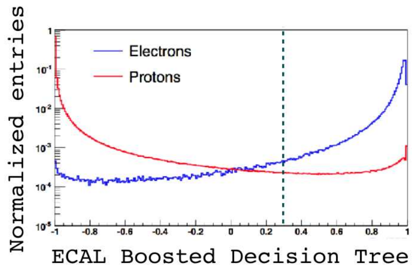

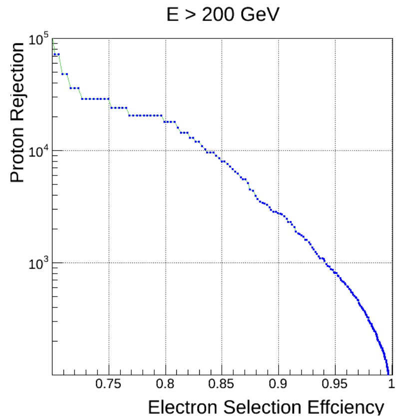

Positron identification with ECAL

electron and proton create different "tracks" in electromagnetic calorimeter (ECAL)

Boost Decision Tree (BDT) folds the different observables that can distinguish both particles, into one cut

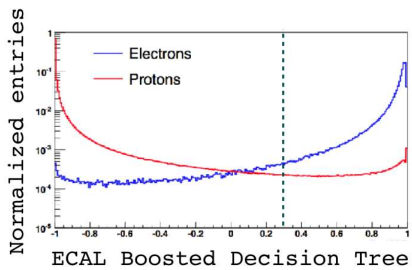

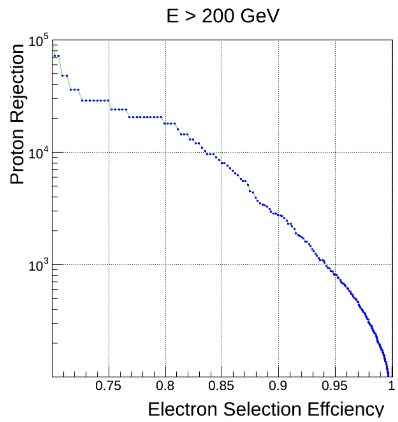

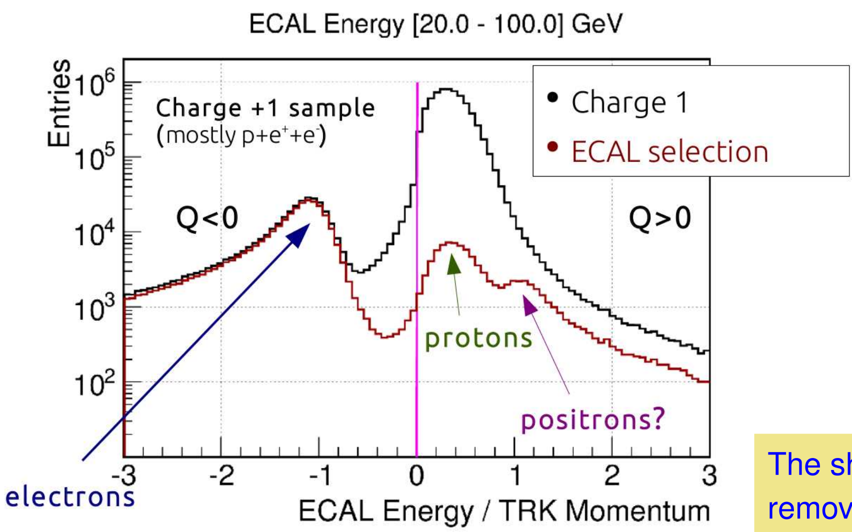

The shower topology (BDT cut >0.3) removes a large fraction of the proton bck while keeping signal

Positron and electron measurement

The number of positrons in every energy bin is obtained :

❒ apply the ECAL shower topology cut (BDT), energy dependent

❒ split sample in negative ($Q < 0$) and positive $Q > 0$ particles

❒ number of positrons and electrons obtained from a fit on the two remaining discrimination observables : **TRD estimator** and E/p

✔ reference spectra from electron and proton samples selected with ECAL

✔ wrong-sign events (charge confusion) spectrum taken into account

Positron and electron measurement

The number of positrons in every energy bin is obtained :

❒ apply the ECAL shower topology cut (BDT), energy dependent

❒ split sample in negative ($Q < 0$) and positive $Q > 0$ particles

❒ number of positrons and electrons obtained from a fit on the two remaining discrimination observables : **TRD estimator** and E/p

✔ reference spectra from electron and proton samples selected with ECAL

✔ wrong-sign events (charge confusion) spectrum taken into account

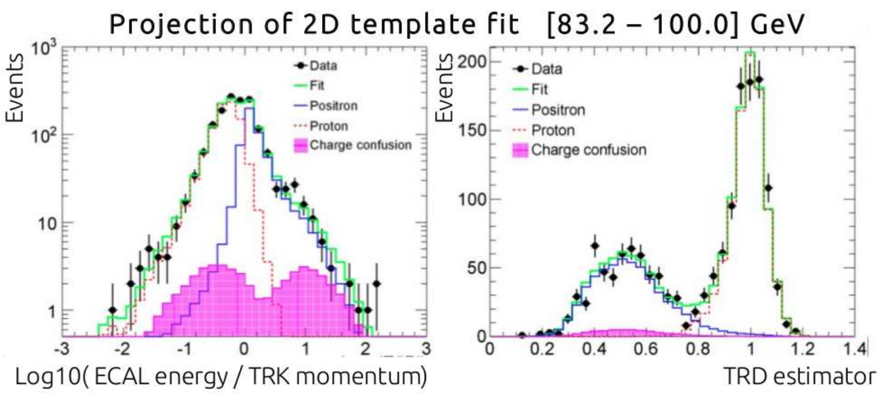

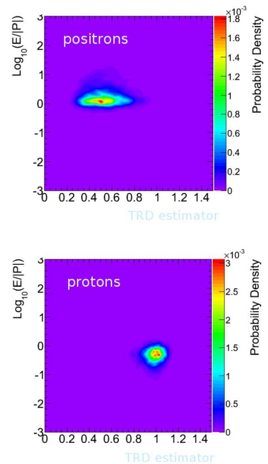

Positron ratio

The positron fraction

$$r_{e^+} = \frac{N_{e^+}}{N_{e^+} + N_{e^-}}$$

2 years of data

$\sim 74000 e^+$ events

72 events on last energy bin (260-350)GeV

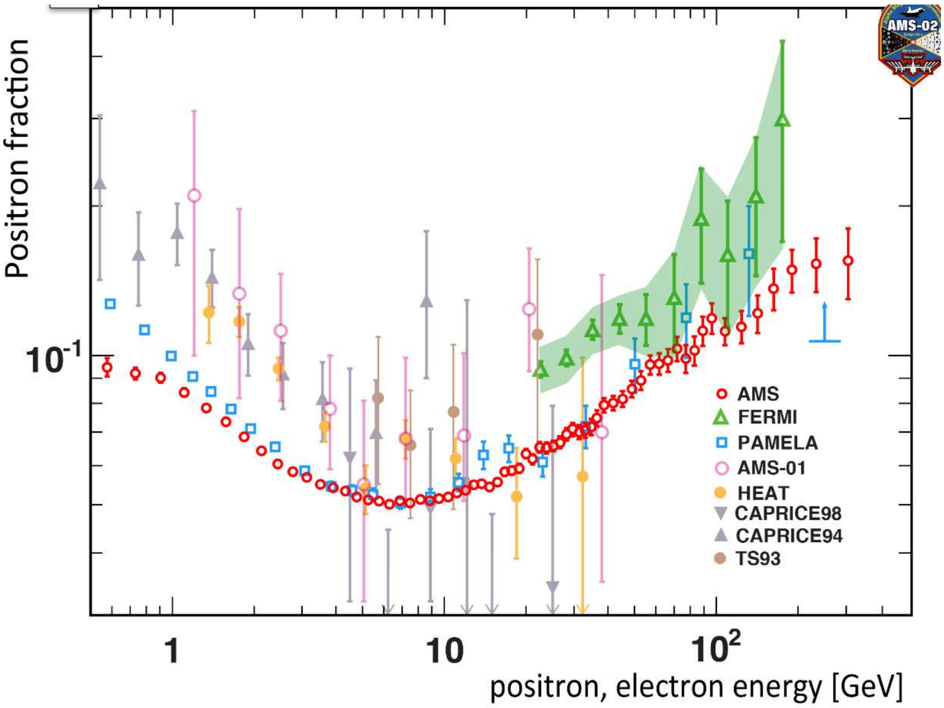

Positron ratio

The positron fraction

$$r_{e^+} = \frac{N_{e^+}}{N_{e^+} + N_{e^-}}$$

2 years of data

$\sim 74000 e^+$ events

72 events on last energy bin (260-350)GeV

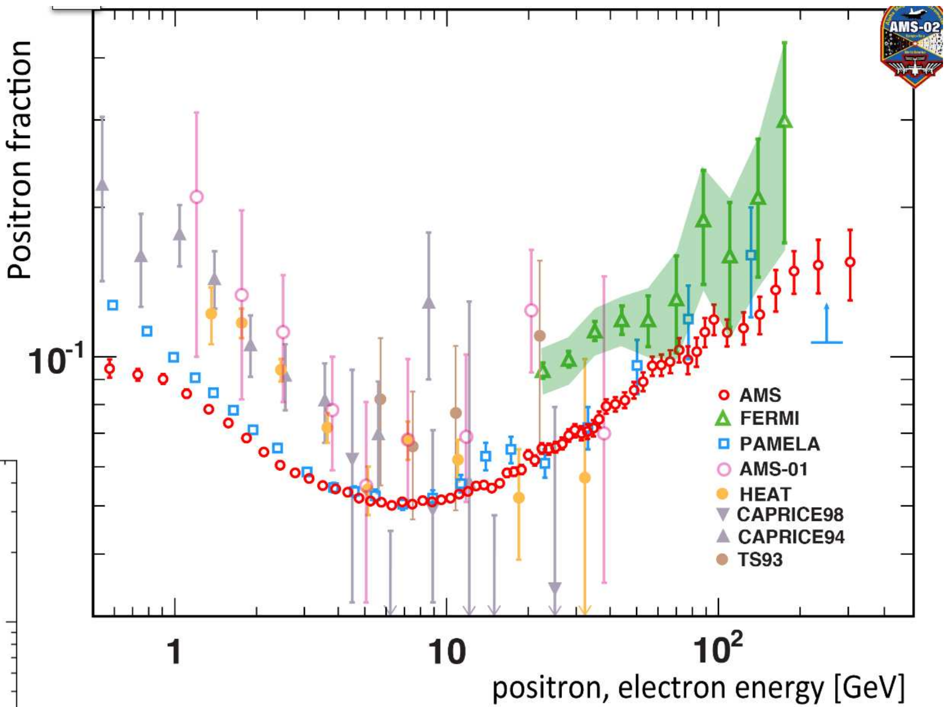

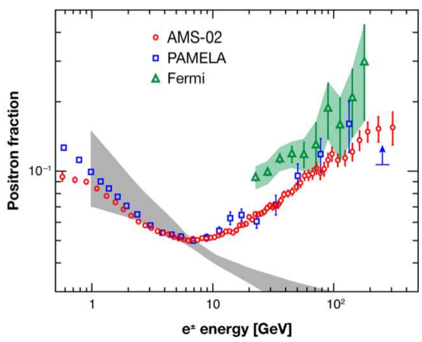

e^+ secondary production is exptected to decrease monotonically while results indicate a persistent rise !

Conclusions

- ✔ 100 years passed since cosmic rays were discovered
- ✔ it has been a long journey with plenty of discoveries (positron, muon, ...) and precise measurements
- ✔ very puzzling questions are still there (P Salati talk) : dark matter, antimatter, a better knowledge of the CR propagation mechanisms...so, better measurements needed to feed theoreticians, phenomenologists !
- ✔ the AMS experiment will remain a fundamental observatory of Cosmic Rays for the next decade
  - ► detailed measurements in energy and charge composition will be made with an unprecedented statistical precision
  - ► better precision...an open window to new physical phenomena !